

Validation of remotely sensed evapotranspiration over the Hai River Basin, China

Zhenzhen Jia,¹ Shaomin Liu,¹ Ziwei Xu,¹ Yujie Chen,¹ and Mingjia Zhu¹

Received 18 October 2011; revised 27 May 2012; accepted 29 May 2012; published 12 July 2012.

[1] Ground-based validation is crucial for ensuring the accuracy of remotely sensed evapotranspiration (RS_ET) and extending its application. This paper proposes an innovative validation method based on multisource evapotranspiration (ET) from ground measurements, with the validation results including the accuracy assessment, error source analysis, and uncertainty analysis of the validation process. It is a potentially useful approach to evaluate the accuracy and analyze the spatiotemporal properties of RS_ET at both the basin and local scales, and is appropriate to validate RS_ET in diverse resolutions at different time-scales. An independent RS_ET validation using such a method was presented over the Hai River Basin in 2002–2009, China. In general, validation at the basin scale showed good agreements between the 1 km annual RS_ET and the validation data such as the water balance ET (root-mean-square error (RMSE): 50.73 mm), MODIS ET products (RMSE: 79.84 mm), precipitation, and land use types. At the local scale, multiscale ET measurements from large aperture scintillometer (LAS) and eddy covariance system (EC) with a footprint model were used for validation over three typical landscapes. In most cases, the 1 km RS_ET resulted in slight overestimation with the LAS measurements (RMSE: 10.75 mm for monthly results, 0.78 mm for daily results), while the 30 m RS_ET was underestimated compared to the EC measurements (RMSE: 16.28 mm for monthly results, 0.99 mm for daily results). Furthermore, error sources of RS_ET and uncertainties of the validation process were investigated in detail. The results showed that the proposed validation method was reasonable and feasible.

Citation: Jia, Z., S. Liu, Z. Xu, Y. Chen, and M. Zhu (2012), Validation of remotely sensed evapotranspiration over the Hai River Basin, China, *J. Geophys. Res.*, 117, D13113, doi:10.1029/2011JD017037.

1. Introduction

[2] Evapotranspiration (ET) is an important component of the surface energy balance and the water cycle. A precise estimation of regional ET is considered essential for the applications, such as global environmental change research, basin-scale water resource management, and sustainable development of agriculture. Many parts of the world are facing a growing water crisis, especially in arid and semi-arid areas. For example, the Hai River Basin in northern China, which is our study area with many competing uses for water, provides water supply to 10% of China's population, including dozens of megacities such as Beijing and Tianjin, but its average annual water resources only accounts for 1.5% of that of the whole country. Water shortage has become one of the most severe problems influencing the sustainably economic and social development of the Hai

River Basin due to the effects of climate change and the overexploitation of water resources (<http://www.hwcc.gov.cn>). Because wise use of water supplies must begin with knowledge of how much water agricultural crops or natural ecosystems actually consume through ET and how that consumption will change as climate patterns change, there is an urgent need to know actual ET.

[3] Fortunately, there have been significantly technical and theoretical advances in our knowledge of ET over the past two decades owing to the technical innovation, synergy between disciplines, and expressed need [Nagler, 2011]. The highly accurate acquisition of the spatiotemporally continuous ET information using remote sensing technology has attracted the attention of researchers and managers. General reviews about various ET estimation models using satellite data can be found in the literatures given by Courault *et al.* [2005], Glenn *et al.* [2007], Kalma *et al.* [2008], Li *et al.* [2009], Allen *et al.* [2011], and Wang and Dickinson [2012]. The well accepted models in many parts of the world can be divided into four main categories: surface energy balance models including one-source models [Bastiaanssen *et al.*, 1998; Su, 2002; Allen *et al.*, 2007] and two-source models [Shuttleworth and Gurney, 1990; Blyth and Harding, 1995; Norman *et al.*, 1995; Anderson *et al.*, 1997]; empirical statistical models

¹State Key Laboratory of Remote Sensing Science, School of Geography, Beijing Normal University, Beijing, China.

Corresponding author: S. Liu, State Key Laboratory of Remote Sensing Science, School of Geography, Beijing Normal University, 19 Xijiekouwai St., Beijing 100875, China. (smlu@bnu.edu.cn)

[Jackson *et al.*, 1977; Di Bella *et al.*, 2000; Wang and Liang, 2008]; the traditional ET estimation approaches combined with remote sensing [Liu *et al.*, 2010a; Fisher *et al.*, 2011; Mu *et al.*, 2011]; and the remote sensing models based on distributions in surface temperature-vegetation index triangle/trapezoid space [Jiang and Islam, 1999, 2001; Wang *et al.*, 2006; Tang *et al.*, 2010].

[4] However, numerous controlling factors are involved in remotely sensed evapotranspiration (RS_ET) estimation due to the complexity of land surface processes, including climate, plant biophysics, soil properties and topography [Mu *et al.*, 2007]. Hence, achieving the RS_ET with confident certainty is required but difficult. The major limitations can be concluded as the following aspects [Kalma *et al.*, 2008; Li *et al.*, 2009; Allen *et al.*, 2011]: (1) model mechanism, including the applicability of the model in different regions and the factors influencing the model, such as local environment, advection, and heterogeneity of the landscape; (2) model inputs, specifically the accessibility and accuracy of model inputs, such as the uncertainties of land surface parameters retrieved from remote sensing and the acquisition of meteorological elements at satellite pixel scale; (3) parameterization schemes, such as the difficulties in the parameterization of dynamic and thermodynamic factors at the regional scale; and (4) scaling issue, especially deriving a long-term RS_ET series (e.g., daily, monthly, annual RS_ET) from instantaneous RS_ET. Because of these uncertainties, it is indispensable to quantitatively assess the accuracy of RS_ET estimates and to measure the errors, which can be beneficial to improve the remote sensing models and is necessary to ensure RS_ET can be confidently used in practice. Researchers have widely recognized the importance of RS_ET validation, but the validation process itself is a complex issue. The scale mismatch between RS_ET and tower observations makes their comparisons difficult and the evaluation of the remotely sensed estimates challenging [Vinukollu *et al.*, 2011b]. Li *et al.* [2009] argued that the lack of the measured ET at satellite pixel scale for the truth validation is one of the problems in ET studies that have not been solved reasonably. Furthermore, the establishment of quantitative assessment methods and evaluation indexes, and the performance of an uncertainty analysis of the validation process are also some of the current challenges in RS_ET validation.

[5] Currently, for the global, continental, and basin-scale estimates, the total amount of long-term accumulated RS_ET (e.g., monthly, annual, or average annual) has been widely validated using the regional ET calculated from the water balance method. Liu *et al.* [2006] calculated the water balance ET over the Yellow River Basin in China for the period 1981–2000 to validate the overall annual RS_ET derived from three different complementary relationship approaches. Ferguson *et al.* [2010] used the GRACE (Gravity Recovery and Climate Experiment) inferred ET estimates from the terrestrial water budget to evaluate the Penman-Monteith (P-M) based RS_ET on seven large U.S. river basins for the period 2003–2006. Glenn *et al.* [2011] reviewed the basin-scale water balance ET studies in Australia, which were used to compare with the long-term RS_ET estimates. Vinukollu *et al.* [2011b] used water balance analysis to compare the monthly RS_ET estimated from three models (i.e., one-source energy balance model,

P-M based and Priestley-Taylor based models) across 26 global river basins for the 2003–2006 period.

[6] For the local or field scales, ground measurements are used to validate RS_ET. The ET measurements can be derived from lysimeter, Eddy Covariance system (EC), Bowen Ratio Energy Balance system (BREB) and scintillometer. Allen *et al.* [2011], Wang and Dickinson [2012] summarized the basic principles, advantages and disadvantages as well as the measurement biases of the above commonly used methods of ET observation. In recent years, many researchers have used these measurements to validate RS_ET. Tasumi *et al.* [2005] and Teixeira *et al.* [2009] verified the rationality of regional RS_ET estimation with SEBAL (Surface Energy Balance Algorithm for Land) based on Landsat TM data using lysimeter, BREB and EC over the Bear River basin in the USA and the Sao Francisco in Brazil, respectively. Kalma *et al.* [2008] summarized 30 cases of ground-based (EC or BREB) validation over different surface types. The data set from the global network (FLUXNET) of more than 500 sites, where tower-based EC provide continuous measurements, is now widely used in the validation of RS_ET [Fisher *et al.*, 2011; Mu *et al.*, 2011; Vinukollu *et al.*, 2011b]. However, as the spatial representativeness of lysimeter, EC and BREB measurements are normally a few to hundreds of meters, such an observation at point or patch scales can be only used to validate RS_ET at fine resolution (e.g., Landsat TM/ETM+, ASTER, and airborne remote sensing data) over relative homogeneous landscapes.

[7] The scintillometer can determine a path-averaged value of the surface heat flux. Particularly, the measurements of Large Aperture Scintillometer (LAS) are integrated over a long transect of approximately 500–5000 m. The LAS improves the spatial coverage compared with other equipment, and it matches the satellite pixel scales better, especially for remote sensing data at coarse resolution (e.g., MODIS, NOAA/AVHRR, AATSR, and GOES). Thus, the measurements of scintillometer have a strong competitive advantage in the RS_ET validation. Watts *et al.* [2000], Hemakumara *et al.* [2003], Jia *et al.* [2003], and Marx *et al.* [2008] derived ground measurements from LAS to validate the results of instantaneous/daily sensible heat flux and daily RS_ET estimated by a one-source energy balance model (SEBAL or SEBS (Surface Energy Balance System)) based on remotely sensed data, such as NOAA/AVHRR, ATSR, and MODIS in Mexico, Sri Lanka, Spain, and Ghana, respectively. Kleissl *et al.* [2009] established an observational network consisting of seven LASs in New Mexico to obtain the surface flux at the kilometer scale, and evaluated the performance of SEBAL using MODIS data.

[8] It is worth noting that the result of RS_ET is arranged pixel by pixel. However, EC and LAS are generally set up at a certain height, and the field of view of the measurements is highly variable. The concept of “footprint” should be introduced here to describe the spatially representative area of flux measurements. By determining the footprint, the range that mainly contributes to the measurement, namely the source area, and the relative contribution within it can be acquired. Furthermore, the source area depends on measurement height, wind direction/velocity, atmospheric stability and the underlying surface conditions. Shown as the analysis of our footprint model (seen in section 2.3.1), the

source area of EC can generally cover approximately several tens of pixels on the Landsat TM thermal images with 30 m resolution, and that of LAS can cover approximately one to ten MODIS thermal pixels with 1 km resolution through the transect. Thus, RS_ET validation is complicated by the scale gap between footprints of existing flux measurement and the pixel area of remote sensing models [Kleissl *et al.*, 2009]. Whether for the observation of EC at the patch scale or for the path-averaged LAS measurements, the in situ measurements which just represented a special area limited the validation of RS_ET, especially over a heterogeneous landscape. Comparing the measured values with a single pixel value directly can result in a large bias in the evaluation results [Brunsell *et al.*, 2011]. As a result, deciding how to select satellite pixels that have the same spatially representative area as the in situ measurements is a fundamental issue in the ground-based. Some studies compared measurements with the value of a single pixel containing the equipment or an arithmetic mean value of pixels within a certain range [Hemakumara *et al.*, 2003; Jia *et al.*, 2003; Marx *et al.*, 2008]. Other investigations showed good results by introducing the footprint model into the validation to solve the mismatch between RS_ET and the measurements [Chávez *et al.*, 2005; Liu *et al.*, 2007a; Kleissl *et al.*, 2009; Brunsell *et al.*, 2011; Song *et al.*, 2012].

[9] The intercomparison of multisource models or products is another option for the validation of RS_ET. Timmermans *et al.* [2007] suggested that although some validation experiments demonstrated that the models yield accurate estimates at the flux measurement sites, the question remains whether they are performing well over the broader landscape. Moreover, it is difficult to assess how generally applicable the models are outside the range of conditions sampled. On the other hand, a large number of RS_ET products have been released in recent years. For example, the MODIS global ET products (MOD16) at 1 km resolutions [Mu *et al.*, 2007; Mu *et al.*, 2011] (details in section 2.3.3), and the daily RS_ET at a global scale and 0.25 degree spatial resolution produced by the VU University, Amsterdam [Miralles *et al.*, 2011]. Consequently, the research on the model or product intercomparison becomes possible and necessary. Vinukollu *et al.* [2011a] pointed that recent evaluations of global estimates from remote sensing, upscaled observations, land surface models, and atmospheric reanalysis indicated large uncertainty across the data sets of the order of 50% of the global annual mean value. Similar studies are always conducted at global and basin scales for validation recently [Jiménez *et al.*, 2011; Mueller *et al.*, 2011]. Some other intercomparisons were made focusing on the remote sensing models, which usually performed at basin or local scales. French *et al.* [2005] and Tang *et al.* [2011] intercompared the one source and two source energy balance models combined with in situ flux measurements. Gao and Long [2008] used a SVAT-based (Soil-Vegetation-Atmosphere Transfer schemes) ET to compare the daily RS_ET estimated from four different energy balance models in the upper Chao river. Ferguson *et al.* [2010] utilized the simulations from a macroscale hydrology model to quantify the spatiotemporal properties of RS_ET derived from a P-M model over continental USA.

[10] With the support of the World Bank and the Chinese government, the Global Environment Facility (GEF) has

funded the Integrated Water and Environment Management Project at the Hai River Basin in China since 2004, aiming to improve the basin-scale water resources and water environment management to effectively alleviate the shortage of water resources. A new technique of water resources planning and management based on satellite remote sensing, namely “ET management,” has been introduced in this project to reduce the current ET values over the basin to a sustainable level. In the GEF Hai River project, RS_ET data are produced using the ETWatch system [Wu *et al.*, 2011] by the Institute of Remote Sensing Applications in Chinese Academy of Science. Meanwhile, to ensure the accuracy of RS_ET and improve confidence in the application of RS_ET products, an independent ground-based validation was undertaken by our research group in Beijing Normal University.

[11] Taking into account the above mentioned importance and problems of RS_ET validation, the objective of this paper was to propose an innovative validation method of RS_ET at different temporal and spatial scales by using multisource validation data sets. For this purpose, the in situ flux sites with LAS and EC observations over three typical landscapes were established to obtain multiscale ET measurements over the Hai River Basin since 2007. Subsequently, a relatively systematic validation procedure was addressed, including accuracy assessment, error source analysis, and uncertainty analysis of the validation process. To solve the problem of spatial match between RS_ET and in situ measurements, we focused on the acquisition of multiscale ET measurements and the selection of validation pixel integrated with the footprint model. An independent validation of a long-term RS_ET series (30 m and 1 km resolutions) over the Hai River Basin was conducted at both the basin and local scales to evaluate the performance of the proposed validation method.

2. Data

2.1. Study Area

[12] The Hai River Basin (Figure 1) is located at 112.0°E–119.8°E, 35.0°N–42.8°N. The basin has an area of 318,000 km², and the elevation ranges from 100 to 3000 m, increasing from southeast to northwest. The north and west parts of the basin are dominated by mountains and plateaus, accounting for 60% of the whole area. The east and southeast parts are mainly the North China Plain, which is nearly 40% of the whole area. Winter wheat is rotated with summer maize over the basin (<http://www.hwcc.gov.cn>). A land use map of the basin is shown in Figure 1.

[13] The Hai River Basin is a continental semi-humid and semi-arid area in the temperate monsoon zone. For the period of 1960–1999, the average annual temperature was 10.4°C, and the average annual precipitation was 541.6 mm, which commonly occurred between June and September and had an uneven spatial distribution [Yuan *et al.*, 2009].

2.2. Remotely Sensed Data Set

[14] Landsat TM data and MODIS products (including MOD021KM, MOD02QKM, MOD02HKM and MOD03) were used in this study. The 250 m resolution MOD02QKM and 500 m resolution MOD02HKM products were both aggregated to 1 km resolution. Meteorological elements

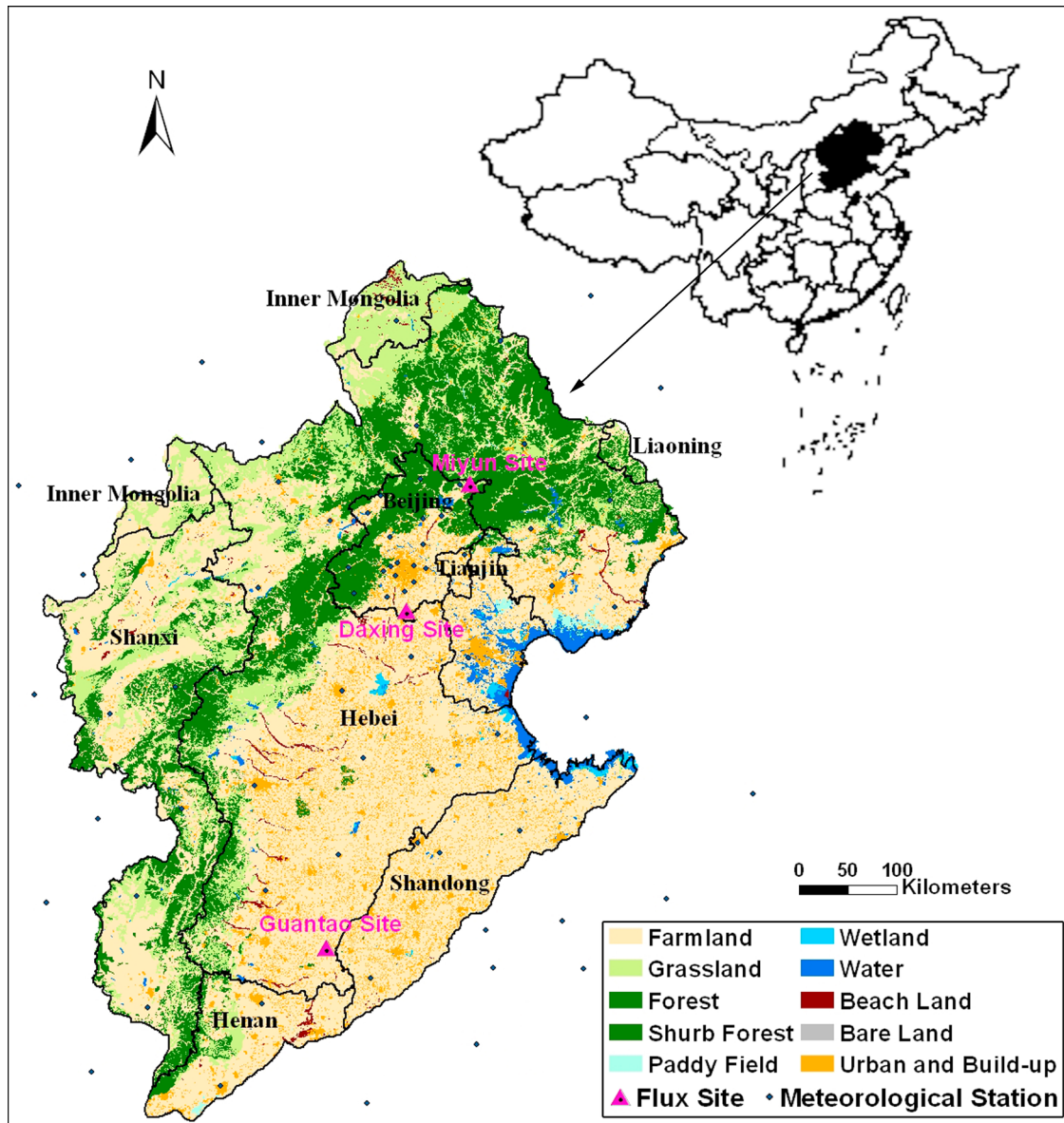


Figure 1. The location and land use of the Hai River Basin in China. The triangle represents the flux site with the name marked, and the black point represents the meteorological station. The black line is the provincial boundary and the name of the province is marked on the map.

including wind speed, air temperature, daily maximum and minimum air temperature, relative humidity, air pressure and percentage of sunshine were collected from 83 meteorological stations (shown in Figure 1) located over the Hai River Basin [Xiong *et al.*, 2010]. All the information was interpolated into daily maps at 1 km resolution, using the inverse distance squared method for air temperature and air pressure in combination with DEM (Digital Elevation Model) data, whereas the thin plate spline method for others, and then was resampled to 30 m resolution. In addition, the land use classification map was acquired combining the method of supervised classification with visual interpretation based on MODIS visible and near infrared bands at 250 m resolution.

[15] Daily, monthly and annual RS_ET over the Hai River Basin at 1 km resolution and those of 16 counties at 30 m resolution from 2002 to 2009 have been estimated by the

ETWatch system. In this study, the validated RS_ET data including: (1) annual RS_ET (1 km) during 2002–2009, daily and monthly RS_ET (1 km and 30 m) during 2007–2009, and (2) model variables (1 km) such as daily net radiation, instantaneous evaporative fraction and surface resistance during 2008–2009.

2.3. Validation Data Set

2.3.1. In Situ Flux Data at Multiscale

[16] In situ flux measurements were collected from three sites in 2007–2009 over the Hai River Basin, namely the Miyun, Daxing and Guantao sites (Figure 1). To validate the RS_ET over the basin, ground-based sites were established over three typical landscapes which were the major types in the Hai River Basin: the Miyun site ($40^{\circ}37'50.8''\text{N}$, $117^{\circ}19'23.8''\text{E}$) is located in the northern mountain area of the basin,

with a surface mainly covered by orchard and maize; the Daxing site (39°37'16.7"N, 116°25'37.2"E) is located in the middle reach of the basin over the suburban farmland of Beijing, with main crops of winter wheat/maize and vegetables; and the Guantao site (36°30'54.1"N, 115°07'38.7"E) is located in the North China Plain and is mainly planted with winter wheat/maize and cotton. At each site, an observation system consisting of EC, LAS and Automatic Weather Station (AWS) was set up to acquire the flux measurements and accessorial parameters at both the hectometer and kilometer scales simultaneously. It is worth noting that as the LAS footprint typically takes an ellipsoid shape, whose major axis is approximately 30% less than the actual path length [Kleissl *et al.*, 2009], the LAS transects need to cover more than one-and-a-half of the MODIS pixels (1 km resolution). Thus, the path length of LAS at all three sites in this study was designed longer than two kilometers. EC and AWS are located in the center of the LAS path (only at the transmitter side of LAS at Daxing site). Then the remote sensing estimates at different resolutions can be validated by utilizing these data sets in combination with the footprint model. A summary of the instruments and the surface characteristics at the three validation sites are given in Table 1. All of the above measured data of EC, LAS, and AWS were rigorously and carefully processed following the uniform standard procedures [S. M. Liu *et al.*, 2011].

[17] Half-hour EC measurements were obtained from the raw data sampled at 10 Hz with the post-processing software EdiRe (University of Edinburgh, <http://www.geos.ed.ac.uk/abs/research/micromet/EdiRe>). Because of the energy imbalance of EC (the energy balance ratio was in the range of 0.76–0.91 at the three sites during 2007–2009), a calibration of energy closure for the sensible and latent heat fluxes measurements derived from EC was made based on a Bowen ratio closure method [Twine *et al.*, 2000]. In addition, the missing data due to instrument malfunction, poor maintenance, and bad weather conditions were gap-filled by the look-up table method and the mean diurnal variations method [Falge *et al.*, 2001], after which the ET series at different temporal scales (daily, monthly and annual) could be obtained.

[18] For the LAS measurements, rigorous data screening was executed for the raw data (structure parameter of the refractive index of air, C_n^2) first, including the rejection of data obtained during the periods of precipitation, data beyond the saturation criterion, data with small demodulated signals, data in weak turbulence condition during night, and data when the sensor was malfunctioning. Strictly speaking, C_n^2 is related to the temperature structure parameter C_T^2 , the humidity structure parameter C_q^2 , and a covariant term C_{Tq} . Because the optical scintillometer is more sensitive to temperature variations than humidity, as a simplification, C_n^2 is related to C_T^2 directly in our study, as proposed by Wesely [1976]. Then the sensible heat flux could be obtained in combination with the meteorological data based on Monin-Obukhov similarity theory (MOST) [Mejninger *et al.*, 2002a]. According to the usual method that LAS data quality was judged by comparing with MOST theory value [Hoedjes *et al.*, 2007], the measurements at all three sites were closed to the theory line, that is to say, the LAS data used in our analysis were in good quality [Liu *et al.*, 2010b].

Moreover, the missing data at 30 min intervals were gap-filled using a nonlinear regression method [Berbigier *et al.*, 2001] for unstable conditions, while taking the data under stable conditions as zero. For the missing data of daily sensible heat flux, a dynamic linear regression method [Alavi *et al.*, 2006] was used for interpolation. Finally, the daily ET from the LAS observation was acquired according to the energy balance equation combined with the measurements of surface net radiation and soil heat flux [Mejninger *et al.*, 2002a].

[19] The meteorological elements observed by AWS are listed in Table 1. A small amount of data which obviously beyond the physical meaning were rejected and then gap-filled by a linear interpolation method. It is worth noting that because the soil heat flux plates were buried at depths of 0.02 m at the validation sites, the surface soil heat flux was calculated using the method proposed by Yang and Wang [2008], which is a temperature prediction-correction method based on the thermal exchange equation using the profile of soil temperature and moisture observations.

[20] For RS_ET validation, it is essential to compare RS_ET with measurements originating from identical areas, so the source area of the EC and LAS measurements using the footprint model is required. In this study, an Eulerian analytic flux footprint model was used to obtain the flux footprint, $f_{EC}(x, y, z_m)$, for the EC measurements at a single point, as follows [Kormann and Meixner, 2001]:

$$f_{EC}(x, y, z_m) = D_y(x, y) f^y(x, z_m) \quad (1)$$

where x is the downwind distance pointing against the average horizontal wind direction, y is the crosswind wind distance, z_m is the measurement height of EC, $f^y(x, z_m)$ is the crosswind integrated footprint, and $D_y(x, y)$ is the Gaussian crosswind distribution function of the lateral dispersion.

[21] For the LAS measurements, the flux footprint, $f_{LAS}(x, y, z_{eff})$, was calculated by combining the path-weighting function of LAS with the above point flux footprint function, expressed as [Mejninger *et al.*, 2002b]:

$$f_{LAS}(x, y, z_{eff}) = \int_{x_2}^{x_1} W(x') f(x' - x, y' - y, z_{eff}) dx' \quad (2)$$

where $W(x')$ is the path-weighting function of the LAS; x_1, x_2 are the locations of the LAS transmitter and receiver; x', y' are the points along the optical length of the LAS; x, y are the coordinates upwind of each point (x', y'); and z_{eff} is the effective measurement height of LAS. To obtain the daily and monthly flux source area of the EC and LAS measurements, daily and monthly footprints were determined by averaging every half-hour footprint when the sensible heat fluxes were larger than zero. Values ranging from 22:00 to 6:00 BST (Beijing Standard Time) were also excluded.

[22] In addition, ground measurements of model variables such as evaporative fraction and surface resistance were involved in RS_ET validation. Instantaneous evaporative fraction (EF_{ins}) was estimated using the measurements of latent heat flux (LE), net radiation (R_n) and surface soil heat flux (G_0), as follows:

$$EF_{ins} = LE / (R_n - G_0) \quad (3)$$

Table 1. Summary of the Instruments and the Surface Characteristics at the Three Validation Sites^a

Instrument	Observed Items	Sensor Type	Miyun Site Height/Depth (m)	Daxing Site Height/Depth (m)	Guantao Site Height/Depth (m)
EC	Sensible and latent heat flux	Li7500 and CSAT3, Li-cor and Campbell	26.66	3	15.6
LAS	Sensible heat flux	LAS, Kipp and Zonen	35.86 (path length: 2420 m)	27 (path length: 2480 m)	15.6 (path length: 2760 m)
AWS	Air temperature/humidity	HMP45C, Vaisala	10.66 and 30.56	10 and 27	4 and 12.5
AWS	Wind speed/direction	WS03001, R.M.Young	10.66 and 30.56	27	12.7
AWS	Infrared temperature	IRT-C-3, Avalon	30.56	28	15.7
AWS	Net radiation	CNRI, Kipp and Zonen	30.76	28	15.7
AWS	Soil heat flux	MY/DX: HFT-3, Campbell GT: HFP01, Hukseflux	0.02	0.02	0.02
AWS	Soil temperature profile	AV-10 T, Avalon	0, 0.02, 0.05, 0.1, 0.2, 0.4, 0.6, 0.8, 1	0.02, 0.05, 0.1, 0.2, 0.4, 0.6, 0.8, 1	0, 0.02, 0.05, 0.1, 0.2, 0.4, 0.6, 0.8, 1
AWS	Soil moisture profile	ECH ₂ O-10, Decagon	0.02, 0.05, 0.1, 0.2, 0.4, 0.6, 1	0.02, 0.05, 0.1, 0.2, 0.4, 0.6, 1	0.02, 0.05, 0.1, 0.2, 0.4, 0.6, 1
AWS	Precipitation	MY: 52203, R.M.Young DX/GT: TE525, Campbell	31.46	30	16
AWS	Air pressure	MY: AV-410, Avalon DX/GT: CS100, Campbell	—	—	—
Characteristic					
Starting time			Miyun Site	Daxing Site	Guantao Site
Elevation (m)			2006.08	2007.08	EC/AWS: 2008.01 LAS: 2008.05
Landscape			350	20	30
Maximum Vegetation Height (m)			Orchard, Maize Orchard (plum/apple tree): 4 Maize: 2.2	Winter wheat/Maize, Vegetable Maize: 2.2 Winter wheat: 0.7 Vegetable: 0.5	Winter wheat/Maize, Cotton Maize: 2.2 Winter wheat: 0.7 Cotton: 1.2

^aMY: Miyun, DX: Daxing, GT: Guantao; LAS: Large Aperture Scintillometer, EC: Eddy Covariance system, AWS: Automatic Weather Station.

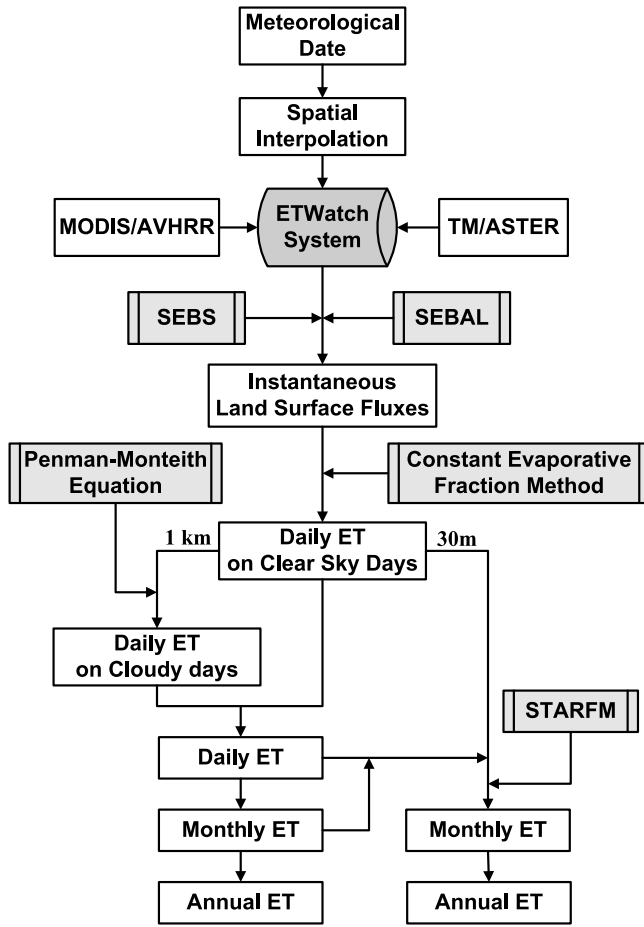


Figure 2. The flowchart of the remote sensing model (ETWatch system). ET: evapotranspiration; SEBS: Surface Energy Balance System; SEBAL: Surface Energy Balance Algorithm for Land; STARFM: Spatial and Temporal Adaptive Reflectance Fusion Model.

half-hour LE from EC and LAS are used here for the validation of remotely sensed EF_{ins} at 30 m and 1 km resolutions, respectively. Then, the daytime evaporative fraction (EF_{day}) is obtained by averaging the EF_{ins} from 9:00 to 15:00 BST.

[23] The calculated value of daily surface resistance (r_{s_cal}) was derived from the LAS and AWS measurements based on the P-M equation [Monteith, 1965]:

$$r_{s_cal} = \left[\frac{\Delta(R_n - G_0) + \rho C_p (e_s - e_a)/r_a}{LE} - \Delta - \gamma \right] \cdot r_a / \gamma \quad (4)$$

where Δ is the slope of the saturation vapor pressure to air temperature, γ is the psychrometric constant, ρ is the air density, C_p is the specific heat of air at a constant pressure, e_a is the actual vapor pressure, e_s is the saturation vapor pressure, and r_a is the aerodynamic resistance. In this study, aerodynamic resistance (r_a) was averaged by the 30-min values considering the stability correction as [Thom, 1975; Liu et al., 2007b]:

$$r_a = \left[\ln \left(\frac{z-d}{z_{0m}} \right) - \psi_m \right] \left[\ln \left(\frac{z-d}{z_{0h}} \right) - \psi_h \right] / k^2 u \quad (5)$$

where z is reference height; z_{0m} and z_{0h} are roughness length for momentum transfer given by Yang et al. [2003] and for heat transfer given by Brutsaert [1982], respectively; d is zero plane displacement height; k was the Karman constant (0.4); u was wind velocity at z ; and ψ_m and ψ_h were the integral forms of the stability correction functions for momentum and heat transfer exchange given by Paulson [1970], Webb [1970], and Businger et al. [1971], respectively.

2.3.2. Hydrologic Data

[24] Regional ET at the basin scale can be estimated by the water balance method, expressed as:

$$ET = P - R + \Delta S \quad (6)$$

where P is precipitation, R is runoff, and ΔS is the change of terrestrial water storage. In this study, R was the difference of water inflow and outflow, and ΔS was evaluated from the groundwater storage and reservoir storage. All the hydrologic data used in the water balance calculation were collected from the Hai River Basin Water Resources Bulletin (<http://www.hwcc.gov.cn>), which recording the data from the hydrological observation network over the basin. The water balance ET over the Hai River Basin during 2002–2009 was calculated according to these data with equation (6). In addition, the spatial distribution of precipitation used in section 4.1.1 was interpolated by the Kriging interpolation method based on the data from 72 meteorological stations which have the long-term rainfall records and are included in Figure 1.

2.3.3. MOD16 Products

[25] The MODIS Global Evapotranspiration Project (MOD16) is part of the NASA/EOS project, whose purpose is to estimate the global terrestrial ET from earth land surfaces using satellite remote sensing data. The MOD16 global ET data sets (MOD16_ET) are regular 1 km² land surface ET data sets for the 109.03 million km² global vegetated land areas at 8-day, monthly and annual intervals, which are blank in the regions of water body, wetland, and urban and built-up areas. The MOD16_ET are estimated using Mu et al.'s [2011] improved ET algorithm based on MODIS and global meteorology data and the P-M equation. The annual MOD16_ET products from 2002 to 2009 over the Hai River Basin area were used in this study (<http://www.ntsg.umd.edu/project/mod16>).

3. Methodology

3.1. Remote Sensing Model Description

[26] Remotely sensed ET was estimated from the ETWatch system developed by the Institute of Remote Sensing Application, Chinese Academy of Science, and the flowchart is given in Figure 2. The ETWatch system is an integration of energy balance models and P-M equation [Wu et al., 2011]. The SEBS [Su, 2002] and SEBAL [Bastiaanssen et al., 1998] models are used to estimate the instantaneous fluxes for moderate resolution (1 km) using MODIS/AVHRR data and for high resolution (30 m) using TM/ASTER data, respectively. Both algorithms provide estimates of instantaneous latent heat flux by solving the energy balance equation. The daily RS_ET at both 1 km and 30 m resolutions on clear sky days are obtained with the method of constant

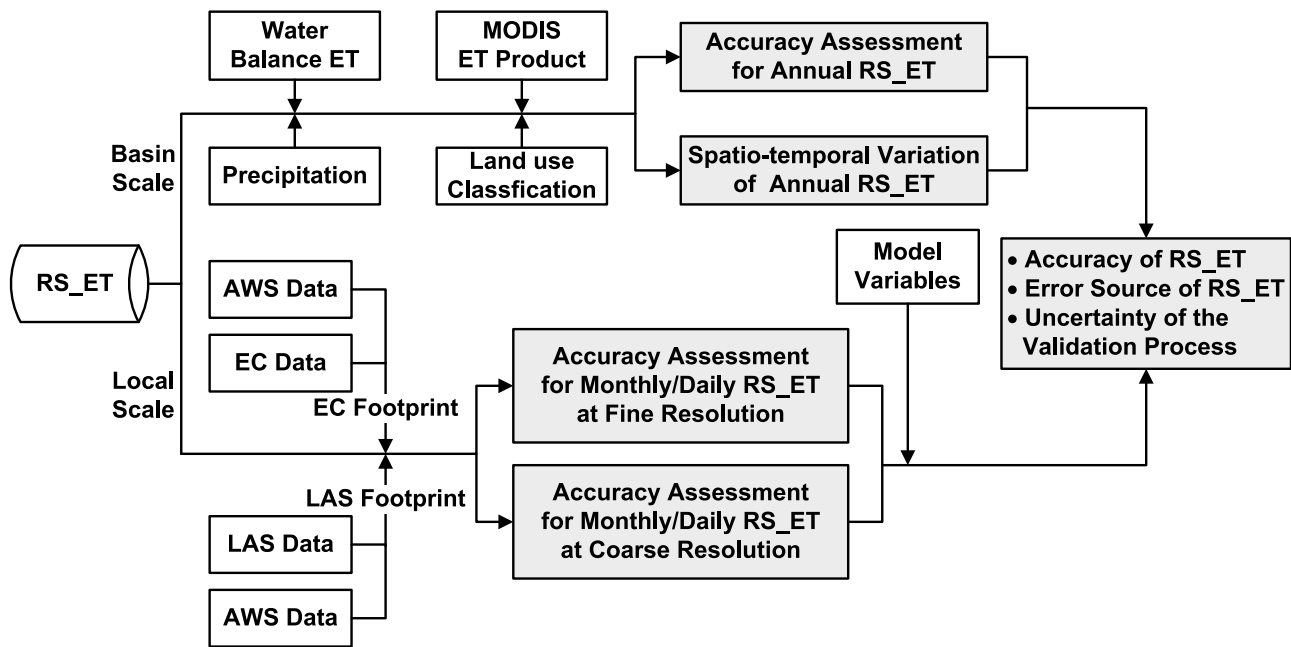


Figure 3. The flowchart of the validation procedure for the remotely sensed evapotranspiration (RS_ET). EC: Eddy Covariance system; LAS: Large Aperture Scintillometer; AWS: Automatic Weather Station.

evaporative fraction, which assuming that evaporative fraction is constant during the daytime. Thus, the daily RS_ET can be retrieved from the daily available energy and the evaporative fraction at the time of satellite overpass. In this study, daily net radiation is calculated as Allen *et al.* [1998] and the daily surface soil heat flux is generally considered as zero.

[27] Spatial and temporal gaps frequently exist in satellite images mainly due to the effect of cloud cover. For example, MODIS provided on average 22% daily clear-sky coverage over the Hai River Basin from 2002 to 2008 [Xiong *et al.*, 2010]. An adequate solution for the intermittent period based on the P-M equation was introduced to generate continuous RS_ET series at 1 km resolution under all sky conditions. Taking advantage of P-M equation (equation (4)), surface resistance on clear sky days ($r_{s,RS,clr}$) is derived from the daily RS_ET inversion. The surface resistance on cloudy days ($r_{s,RS,clr}$) is extended from $r_{s,RS,clr}$ on neighboring clear sky days, Leaf Area Index (LAI), and meteorological elements given by Xiong *et al.* [2010]. Then the daily RS_ET on cloudy days can be obtained by P-M equation.

[28] It is notable that the available data with high resolution data like Landsat TM are much less in a year. In order to get the monthly RS_ET at 30 m resolution, a Spatial and Temporal Adaptive Reflectance Fusion Model (STARFM) [Gao *et al.*, 2006] is introduced. The 30 m monthly RS_ET can be predicted by this data fusion technique between the monthly and daily RS_ET at 1 km resolution and the daily RS_ET at 30 m resolution [S. F. Liu *et al.*, 2011].

3.2. Validation Method

[29] A validation for RS_ET should include three parts: accuracy assessment of RS_ET, error source analysis, and uncertainty analysis of the validation process. For this purpose, on the basis of the acquisition of in situ measurements at multiscale combined with a footprint model (introduced in

section 2.3.1), a validation procedure was proposed in this section.

[30] The validation procedure was composed of validation at the basin and local scales, as illustrated in Figure 3. For the basin scale, the accuracy of the annual RS_ET was evaluated with ET from the water balance method. Meanwhile, the temporal variation was analyzed comparing with the water balance ET and MOD16_ET. Then, the characteristics of the spatial distribution of RS_ET over the basin were discussed, combining with the precipitation data and land use classification map. Spatial differences between RS_ET and MOD16_ET were also evaluated. For the local scale, monthly and daily RS_ET were validated using the in situ measurements over the typical landscapes. Taking into account the inconsistent spatial scales between RS_ET and the measurements, the RS_ET at fine resolution (e.g., at the TM scale) was validated using the EC measurement combined with the EC footprint model, while the RS_ET at coarse resolution (e.g., at the MODIS scale) was validated using the LAS measurement combined with the relevant footprint model. Then, associated with the comparison of the estimated model variables and their measurements, the error source of RS_ET was further analyzed. It was significant that uncertainties might be involved in the whole validation process, not only the errors of RS_ET itself. Therefore, the uncertainty analysis for the validation process was an essential step.

3.2.1. Validation Pixel Selection

[31] The source areas of the EC and LAS measurements at the time of satellite overpass on 25 January 2009 and 2 June 2009 at the Guantao site are shown in Figure 4. As depicted in Figure 4, pixels covered by flux source areas were quite different for the EC and LAS measurements at the time of satellite overpass. At the Guantao site, the EC source area was distributed around the observation point, and its shape changed with the wind direction. The main contributing

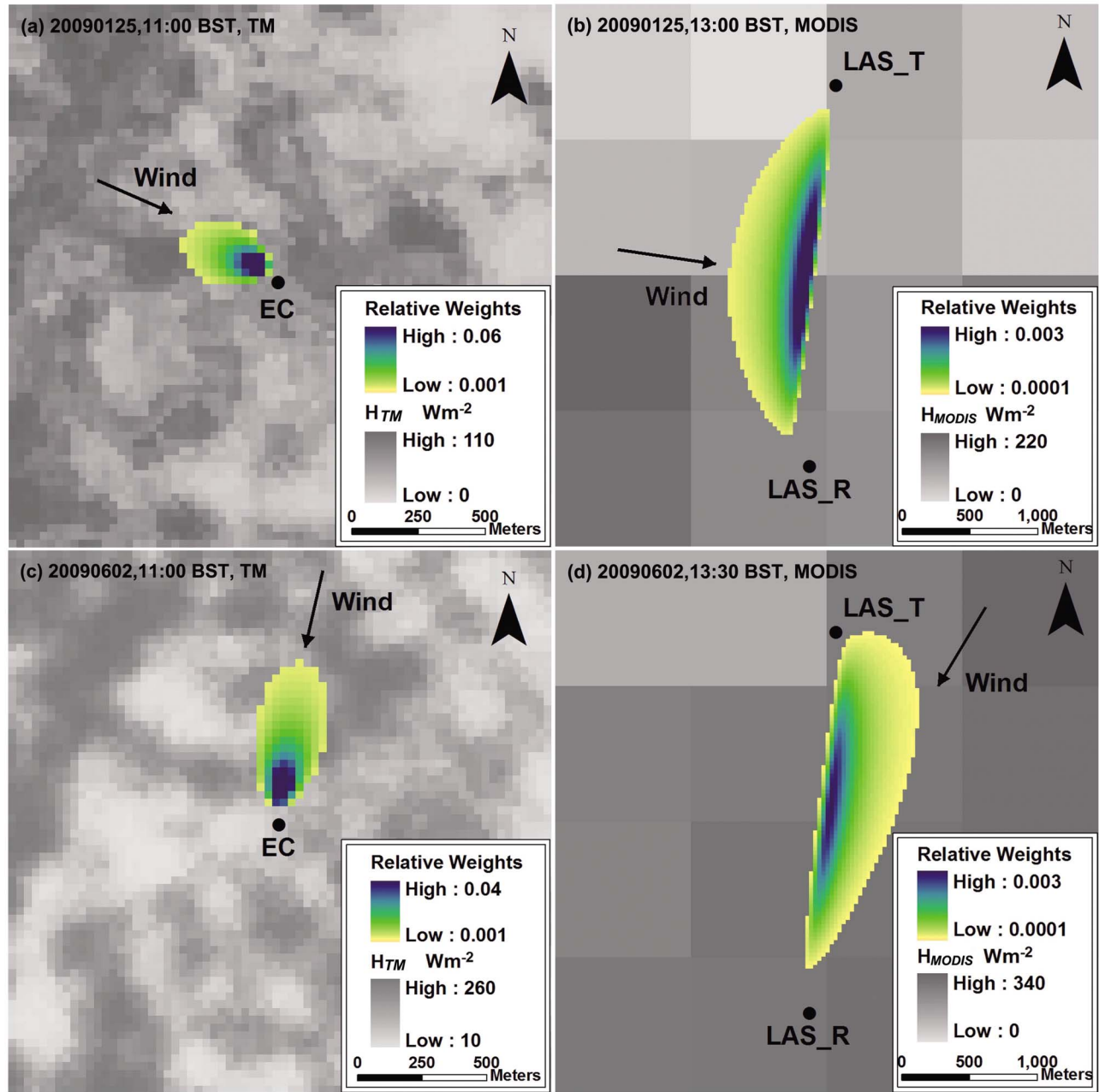


Figure 4. The remotely sensed sensible heat flux (gray-scale images) overlaid with the source areas (colorful images) of EC and LAS measurements at the Guantao site on (left) a TM image and (right) a MODIS image, respectively. (a and b) Images taken on 25 January 2009; (c and d) images taken on 2 June 2009. LAS_T: transmitter of LAS; LAS_R: receiver of LAS.

source areas were approximately 230 m wide and 330 m long on 25 January, 270 m wide and 550 m long on 2 June, which covered 75 and 136 TM pixels, respectively (Figures 4a and 4c). The LAS source area did not show obvious variation, which extended from south to north with the main contributing source areas both being approximately 630 m wide and 2500 m long on the two days. The transect of the LAS source area mainly covered 3 to 4 MODIS pixels (Figures 4b and 4d).

[32] Considering the large variations of the flux source areas and heterogeneity of underlying surfaces, it was

essential to select validation pixels with the help of the footprint model. In this study, the flux source area was calculated within a range of 3×3 km, taking the location of EC and the center of the LAS path as the center of the distribution, respectively, with a grid resolution of 30 m. Then, the footprint function needed to be normalized within the source area to obtain an image of the source area with relative weights. The remotely sensed results from TM and MODIS were overlapped by the footprint-weighted images of EC and LAS, respectively (Figure 4), and pixels within the source area could be taken as the validation pixels. Last,

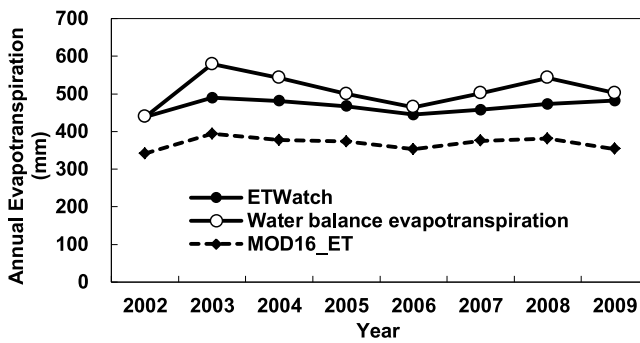


Figure 5. Comparison of the annual evapotranspiration over the Hai River Basin estimated from the ETWatch system, the water balance method and the MODIS product (MOD16_ET) from 2002 to 2009. (Results of the MOD16_ET except the estimation on the surfaces of water body, urban and build-up, and wetland.)

the footprint relative weights, namely the relative contribution, within each pixel were summed up, and the weighted average RS_ET could be computed as:

$$Y_{\text{weighted}} = \sum_{i=1}^n (x_i \times P_i) \quad (7)$$

where Y_{weighted} is regarded as the estimate from remote sensing with the same spatial representativeness as the observation, x_i is the relative weight of each pixel, P_i is the RS_ET value of each pixel, and n is the number of pixels within the source area.

3.2.2. Evaluation Index

[33] Evaluation of model estimation should include the accuracy of results and the consistency of the spatiotemporal variation between estimates and measurements. However, it is difficult to present a complete picture of model performance using a single statistical measure [Rymph, 2004]. For the quantitative analysis of model estimation, a set of evaluation indexes was selected. The mean bias error (BIAS) and the root-mean-square error (RMSE) are usually used to measure the average difference between estimation and observation. The mean relative error (MRE) and the mean absolute percent error (MAPE) both describe the relative extent of deviation of the estimation from observation. The correlation coefficient (Corr.) is used to provide a measure of the consistency or closeness between estimated and measured values. In section 4, RMSE, MRE and Corr. were operated to quantify the accuracy of RS_ET. The calculation method of these evaluation indexes are listed in Appendix A.

4. Validation Results

4.1. Evaluation of RS_ET

4.1.1. Basin-Scale Comparisons

[34] For the basin scale, the annual RS_ET estimated from the ETWatch system over the Hai River Basin at 1 km resolution was compared with that from the water balance method. The average annual RS_ET over the whole basin from 2002 to 2009 was 439, 489, 481, 467, 445, 458, 473, and 482 mm, respectively. The RS_ET was generally lower than the water balance ET with an RMSE of 50.73 mm, an

MRE of -8.31% and a Corr. of 0.90, which indicated a reasonable performance in RS_ET estimation at the basin scale. Besides, the RS_ET was always higher than MOD16_ET with an RMSE, MRE and Corr. of 79.84 mm, 20.21% and 0.72, respectively (the blank pixels in MOD16_ET were not considered).

[35] An interannual comparison of the RS_ET, water balance ET and MOD16_ET over the whole basin in 2002–2009 is demonstrated in Figure 5. Two maximum values in 2003 and 2008 with abundant precipitation and three minimal values in 2002, 2006 and 2009 with insufficient precipitation appeared in the RS_ET. This trend agreed with the water balance ET and MOD16_ET, but the amplitude of RS_ET and MOD16_ET was relatively smooth.

[36] The spatial patterns of annual RS_ET, precipitation and MOD16_ET over the Hai River Basin in 2002–2009 are presented in Figure 6. The spatial patterns of annual RS_ET (Figure 6a) were consistent from year to year, decreasing from southeast to northwest, and they showed good consistency with precipitation (Figure 6b). The precipitation decreased significantly, especially in the northwestern basin, and the RS_ET in this area was, accordingly, lower than results in other regions. By further analysis based on the land use map (Figure 1), we found that the annual RS_ET on the water bodies and wetlands was the largest, more than 700 mm. The RS_ET was generally the highest near the Bohai Bay area of the eastern basin, where the rainfall was relatively abundant and the surface was mostly covered by wetlands and paddy fields. However, in urban areas such as Beijing, Tianjin and other cities, the annual RS_ET was less than 300 mm and the difference between precipitation and RS_ET was large. This phenomenon was resulted from many parts of the urban areas were covered by the impervious surface, and the vegetation coverage fraction was low as well. Besides, most of the precipitation was discharged through the sewers, so the ET was relatively lower and accounted for a small percentage of precipitation. For the vegetation covered area, the annual RS_ET varied from 400 to 700 mm over forest land in the northern basin and mostly over 400 mm in the eastern and southern basin that was mainly covered by farmland. Because of factors such as irrigation, the annual RS_ET was higher than the precipitation on the farmland of the Hai River Basin.

[37] A comparison with the average annual MOD16_ET is shown in Figure 6c. As MOD16_ET was produced at the global scale, the variation of spatial patterns in the MOD16_ET distribution was relatively smoothed, which may be influenced by the input data sets, such as $1^\circ \times 1.25^\circ$ meteorological data and 0.05° albedo data. Thus, the estimation from the ETWatch system was smaller than MOD16_ET in the western and northwest areas, while in the eastern and southeastern plains the estimated values were clearly larger.

4.1.2. Local-Scale Comparisons

[38] For the local scale, both of the monthly and daily RS_ET at 30 m and 1 km resolutions was validated by observation data of the EC and LAS at the Miyun (2007.01–2009.12), Daxing (2008.06–2009.12), and Guantao (2008.01–2009.12) sites. Because of the missing data, the LAS measurements in July 2007 and the EC measurements in March and July 2007 at the Miyun site were not included in this validation. The comparisons for monthly and daily

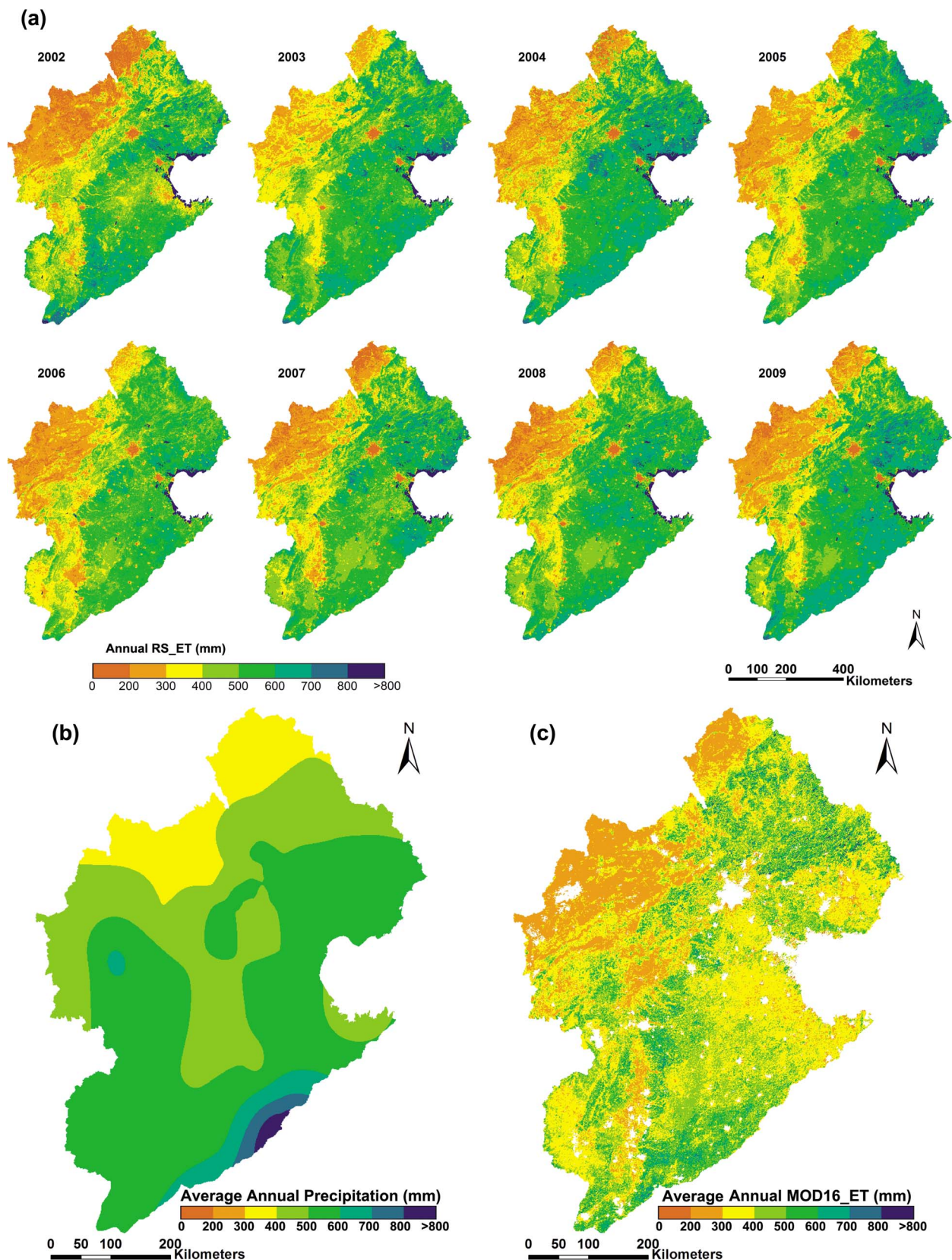


Figure 6. Spatial distributions of (a) the annual remotely sensed evapotranspiration (RS_ET), (b) the average annual precipitation, and (c) the average annual MODIS product (MOD16_ET) over the Hai River Basin from 2002 to 2009. (Blank pixels in MOD16_ET were covered by surfaces of water body, urban and build-up, and wetland with no estimation.)

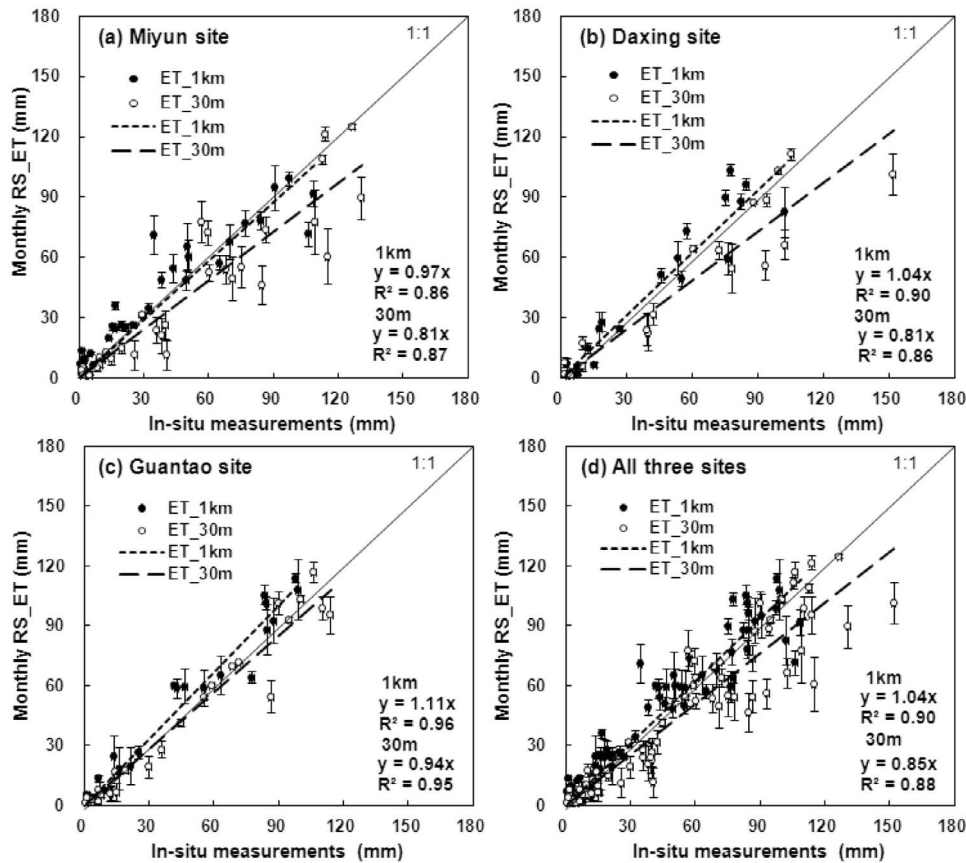


Figure 7. Comparisons of monthly evapotranspiration between the 1 km monthly remotely sensed evapotranspiration (RS_ET) and LAS measurements, and as well as the 30 m monthly RS_ET and EC measurements: (a) Miyun site, 1 km, 30 m: 2007–2009; (b) Daxing site, 1 km: 2008–2009, 30 m: 2007–2009; (c) Guantao site, 1 km, 30 m: 2007–2009; and (d) all three sites. The error bar was calculated as the standard error.

RS_ET with the measurements from the three sites are displayed in Figures 7 and 9, respectively. The accuracy assessment of them is listed in Table 2.

4.1.2.1. Comparisons of Monthly ET

[39] In most cases, the 1 km monthly RS_ET was higher than the measured LAS data from the Miyun, Daxing, and Guantao sites, with the RMSE and MRE being 10.75 mm and 8.32% for all three sites, respectively. The accuracy of the 1 km monthly RS_ET was 88%–95%. During the crop growing seasons, although the deviation (namely RMSE) between estimation and observation was slightly higher than the annual average, the relative value of the deviation, that is, the MRE was almost lower. Compared with the three EC observations, the 30 m monthly RS_ET were mostly smaller with an overall RMSE of 16.28 mm and an MRE of -15.41% , the accuracy of estimation was 80%–92%.

[40] A consistent temporal variation of both monthly RS_ET and in situ measurements at three validation sites is presented in Figure 8, with the Corr. over 0.95 and 0.93 at the 1 km and 30 m resolutions, respectively. Because orchard and maize were planted at the Miyun site, the RS_ET increased gradually along with the temperature increasing and plant growing from April to September, which reached a maximum in July and then decreased as the crop harvested

and orchard withered (Figure 8a). In contrast, crop rotation (winter wheat/summer maize) was adopted at the Daxing and Guantao sites, where the winter wheat was harvested and summer maize began to grow at the end of June. Also, cotton was grown during the period of May to September at the Guantao site. Thus, a bimodal trend was apparent in the seasonal variation of RS_ET at the two sites, which reached the maximum in May and August at the Daxing site, while in May and July at the Guantao site (Figures 8b and 8c).

[41] We found that during the crop growing season, the observed monthly ET from EC was clearly larger than the values from LAS at the Miyun and Daxing sites. On the basis of the analysis of flux source area, the reason for this result was that orchard and maize were contained in the EC source area, while orchard, maize and residential area were included in the LAS source area at the Miyun site. For the Daxing site, the reason was that there was no overlapping source area between the EC and LAS observations, and the amount of irrigation in the EC source area (mainly consisting of winter wheat/summer maize), which is located in an experimental field, was higher than that in the LAS source area (mostly consisting of winter wheat/summer maize, fruits, and vegetables). In contrast, the two types of measurements were close for the Guantao site because both

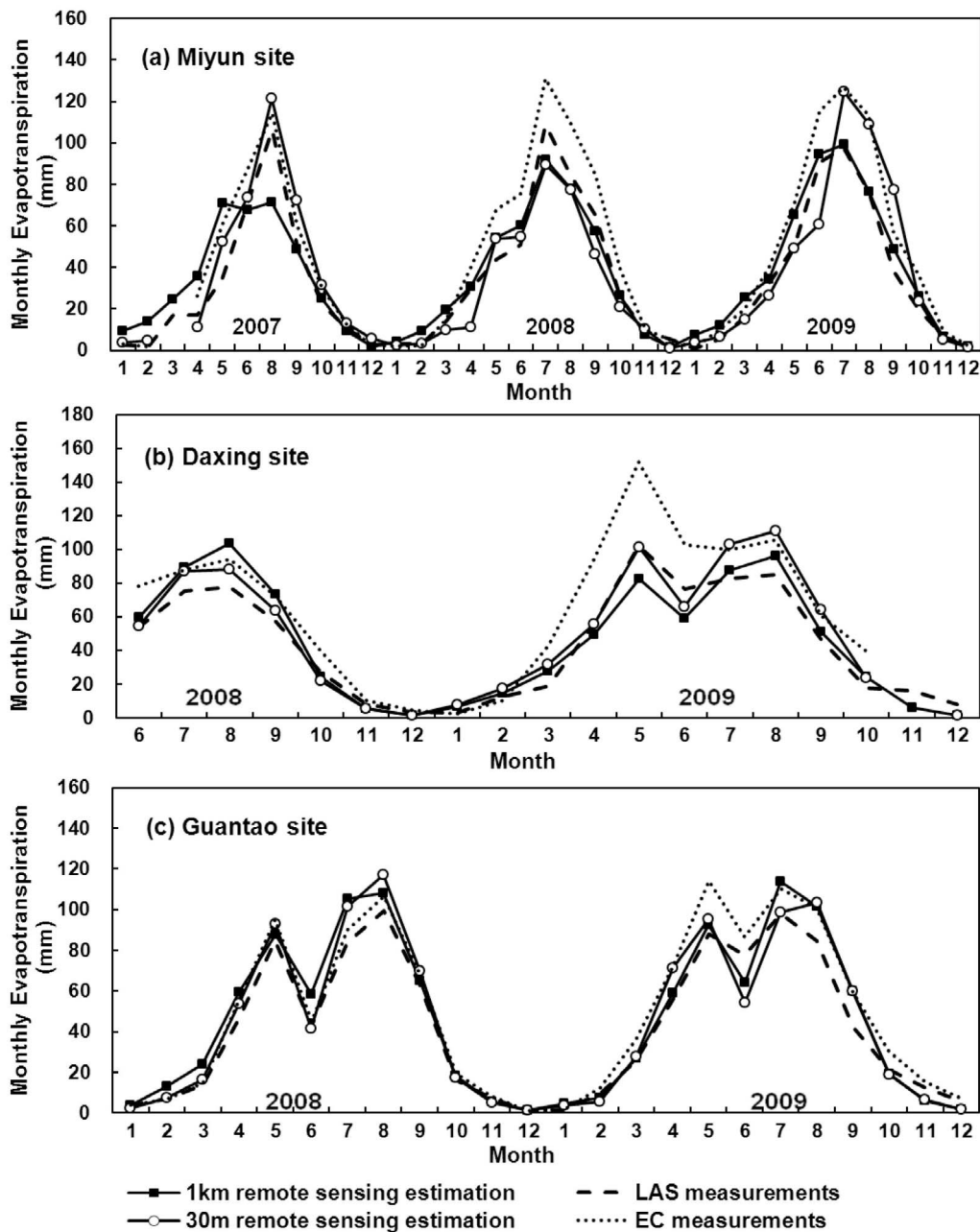


Figure 8. Seasonal variation of the monthly evapotranspiration from remote sensing estimations at 1 km and 30 m resolutions and from the in situ measurements of LAS and EC: (a) Miyun site, 2007–2009; (b) Daxing site, 2008.06–2009.12; (c) Guantao site, 2008–2009.

the EC and LAS source areas were covered by winter wheat/summer maize and cotton. These phenomena could be explained by the heterogeneity of the underlying surfaces and the differences between the source areas of the EC and LAS measurements [S. M. Liu *et al.*, 2011].

4.1.2.2. Comparisons of Daily ET

[42] The 1 km and 30 m daily RS_ET at the Miyun, Daxing, Guantao sites from 2002 to 2009 had been validated, as shown in Figure 9, and 61, 72 and 74 images of MODIS on clear sky days were calculated by the ETWatch system in 2007, 2008 and 2009, respectively. However, because some pixels where the validation sites located in the

satellite image were still affected by cloudy cover or observed data were missing, the actual number of clear sky days involved in the validation of the Miyun, Daxing, Guantao sites was 130, 68, 106 days, respectively. The large deviations were mostly found during the crop growing season, which also affected the consistency between estimates and observations. For the 30 m daily RS_ET estimated from Landsat TM images, 19 clear sky days were validated at Miyun (2007), Daxing (2008–2009), and Guantao (2008–2009) sites. The accuracy assessment of 1 km and 30 m daily RS_ET is listed in Table 2.

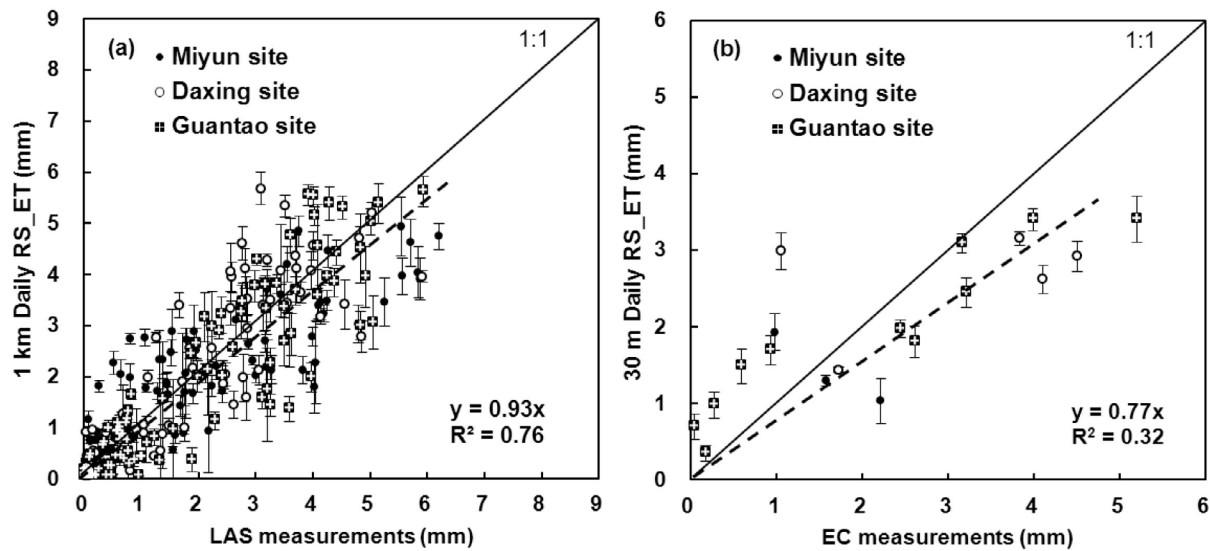


Figure 9. Comparison of the daily remote sensing evapotranspiration (RS_ET) on clear sky days and the measurements: (a) the 1 km daily RS_ET compared with the LAS measurements (Miyun site, 2007–2009; Daxing site, 2008.06–2009.12; Guantao site, 2008–2009) and (b) the 30 m daily RS_ET compared with the EC measurements (Miyun site, 2007; Daxing and Guantao sites, 2008–2009). The error bar was calculated as the standard error.

[43] Overall, for both of the monthly and daily RS_ET estimates at 30 m and 1 km resolutions, the smallest deviation and the most consistent variation trend compared with the measurements were found at the Guantao site, followed by the Daxing and Miyun sites. As known, the Miyun site was located in the mountain area with rolling topography and the Guantao site was located in a flat farmland. So this phenomenon was in agreement with the complexity of underlying surfaces and was influenced by the applicability of the remote sensing models in different regions.

4.2. Error Source Analysis

[44] The validation should not be limited to the accuracy assessment, it is also important to analyze the error sources of the remote sensing estimation, which would further help to understand the estimated results and improve the parameterization of the model. In this section, taking 1 km RS_ET at the Guantao site during 2008 and 2009 as an example, the

error sources were analyzed combined with model variables such as instantaneous evaporative fraction (EF_{ins}), daily net radiation (R_n^{24}), and surface resistance (r_s).

4.2.1. For the Daily Scale

[45] As discussed in section 3.1, the daily RS_ET on clear sky days (Figure 10a) was estimated by the method of constant evaporative fraction, so its accuracy may be related to the accuracy of 1 km R_n^{24} (Figure 10b) and EF_{ins} (Figure 11). As shown in Figure 10b, the R_n^{24} estimation was close to the measurements with an RMSE of 13.48 Wm^{-2} . Figure 11a showed that the temporal variations of estimated EF_{ins} and the in situ measurement were nearly the same, but some deviations could be found in the non-growing seasons of 2008 and 2009. Taking into account the assumption of evaporative fraction daytime self-preservation, the difference between the measured EF_{ins} and daytime evaporative fraction (EF_{day}) was analyzed using the LAS and AWS measurements as presented in Figure 11b. The RMSE was

Table 2. Statistics of the Comparisons Between the Monthly, Daily RS_ET and the LAS, EC Measurements at the Three Validation Sites During 2007–2009^a

RS_ET	Validation Data	Site	Time	RMSE (mm)	MRE (%)	Corr.
1 km Monthly	LAS	MY	2007–2009	11.24 (15.04)	8.41 (3.55)	0.95 (0.85)
	LAS	DX	2008.06–2009.12	11.05 (14.27)	4.31 (5.39)	0.95 (0.70)
	LAS	GT	2008–2009	9.72 (13.00)	11.56 (12.44)	0.98 (0.90)
	LAS	MY, DX, and GT	2007–2009	10.75 (14.24)	8.32 (6.98)	0.95 (0.83)
30 m Monthly	EC	MY	2007–2009	18.06 (24.85)	−19.58 (−19.52)	0.93 (0.82)
	EC	DX	2008.06–2009.12	19.55 (24.65)	−17.67 (−16.14)	0.93 (0.61)
	EC	GT	2008–2009	9.52 (12.24)	−7.59 (−4.49)	0.98 (0.87)
	EC	MY, DX, and GT	2007–2009	16.28 (21.70)	−15.41 (−14.03)	0.94 (0.79)
1 km Daily	LAS	MY, DX, and GT	2007–2009	0.78 (1.03)	0.99 (−1.13)	0.88 (0.71)
30 m Daily	EC	MY, DX, and GT	2007–2009	0.99 (1.02)	−9.09 (−22.99)	0.84 (0.81)

^aNumbers in parentheses are the statistics during growing seasons (April–September). MY: Miyun, DX: Daxing, GT: Guantao; LAS: Large Aperture Scintillometer, EC: Eddy Covariance system.

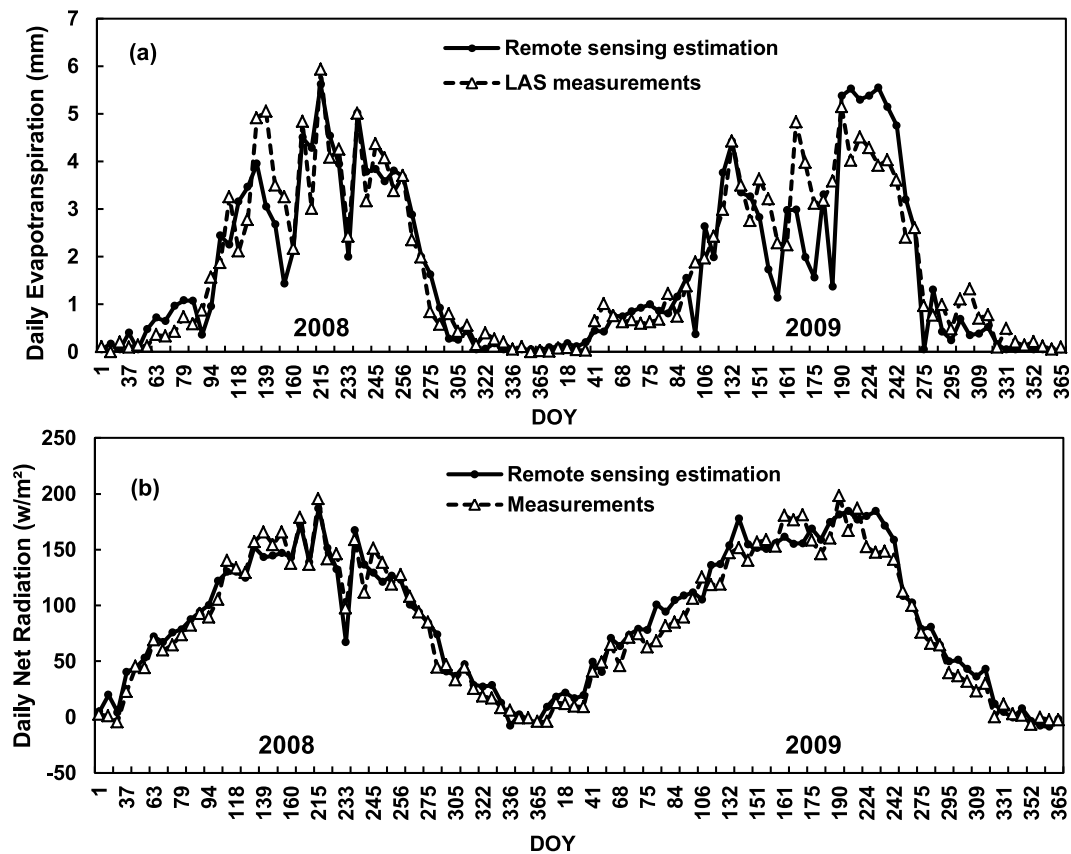


Figure 10. Comparisons of (a) daily evapotranspiration and (b) daily net radiation between the remote sensing estimations and the measurements on clear sky days (Guantao site, 2008–2009).

0.09, which agreed with the point by *Hoedjes et al.* [2008] that many theoretical derivation and experimental studies had shown that the assumption of constant evaporative fraction was not straightforward. *Allen et al.* [2007] also argued that the assumption of the constant evaporative fraction can underpredict the daily RS_ET in arid climates where afternoon advection or increased afternoon wind speed may increase ET in proportion to the available energy. In addition, the fluctuation of the daily RS_ET was found to correspond with the estimated EF_{ins} , and when large deviations of remotely sensed EF_{ins} was seen in Figure 11a, an obvious bias of daily RS_ET could be found on the same day in Figure 10a. Therefore, it was concluded that the errors of the 1 km daily RS_ET mainly came from the estimation errors of remotely sensed EF_{ins} and the assumption of constant evaporative fraction.

4.2.2. For the Monthly Scale

[46] The 1 km monthly RS_ET was obtained by accumulating the daily RS_ET, including the estimated RS_ET based on SEBS on clear sky days and the gap-filled values on cloudy days. Hence, the accuracy of 1 km monthly RS_ET was directly affected by the precision of the daily RS_ET on both clear sky and cloudy days and the number of clear sky days. It was realized that the error source of daily RS_ET on clear sky days was mainly from the estimation of EF_{ins} in section 4.2.1, so the following section will focus on the analysis of RS_ET on cloudy days, which was calculated based on the P-M equation (as pointed out in section 3.1). According to the P-M equation, the accuracy of RS_ET on

cloudy days depended on the daily net radiation, surface resistance, and meteorological elements. The estimation of R_n^{24} achieved good results as seen in Figure 10b. Regarding the meteorological elements, data from 83 meteorological stations were interpolated to a grid at 1 km resolution. Therefore, the performance of the spatial interpolation of the meteorological elements was one of main factors affecting the daily RS_ET estimation on cloudy days.

[47] The difference between remotely sensed surface resistance (r_{s_RS}) and the calculated surface resistance derived from the LAS and AWS measurements (r_{s_cal}) in the growing seasons in 2009 is shown in Figure 12. Early and late in the crop growing seasons, for example, in April and September, most of the r_{s_RS} were underestimated. From January to March and October to December, the estimation of r_{s_RS} was unacceptable because the results appeared as zero or beyond the maximum value of 1000 s/m (not marked in Figure 12). The overall trend of r_{s_RS} and r_{s_cal} was consistent during the crop-growing season. However, taking the precipitation into account, the r_{s_cal} could better reflect the variation of the soil moisture than the r_{s_RS} . From the previous analysis, we learned that the RMSE of 1 km monthly RS_ET at the Guantao site during the whole year of 2009 was 2.83 mm, but the estimated bias (13.72 mm) of monthly RS_ET in June was much larger. Due to the larger amount of precipitation falling in the first ten days of June, a large fluctuation of r_{s_cal} in June was seen in Figure 12 as the soil moisture varied significantly. However, as a result of the influence of soil moisture was not taken into account enough

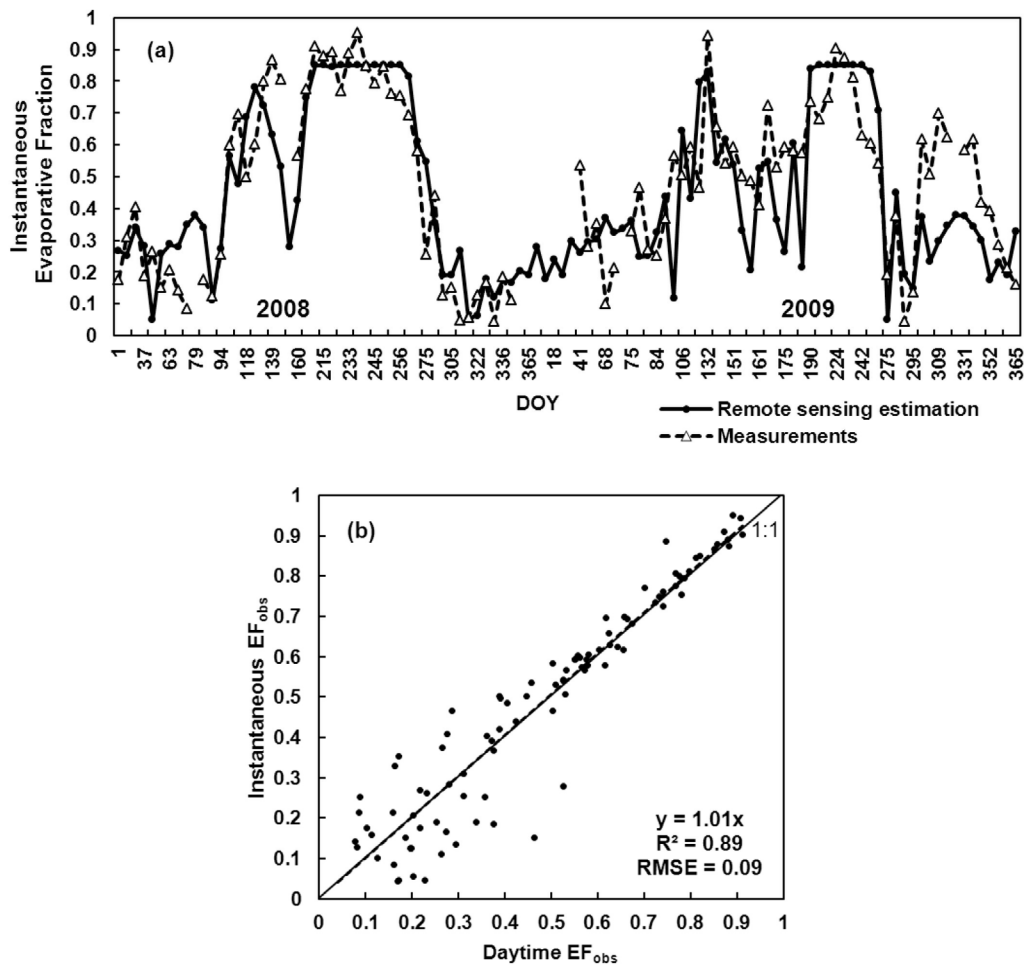


Figure 11. (a) The instantaneous evaporative fraction derived from remote sensing compared with the measurements; (b) comparison of the measured evaporative fraction (EF_{obs}) between the instantaneous values at the time of satellite overpass and the daytime values (Guantao site, 2008–2009).

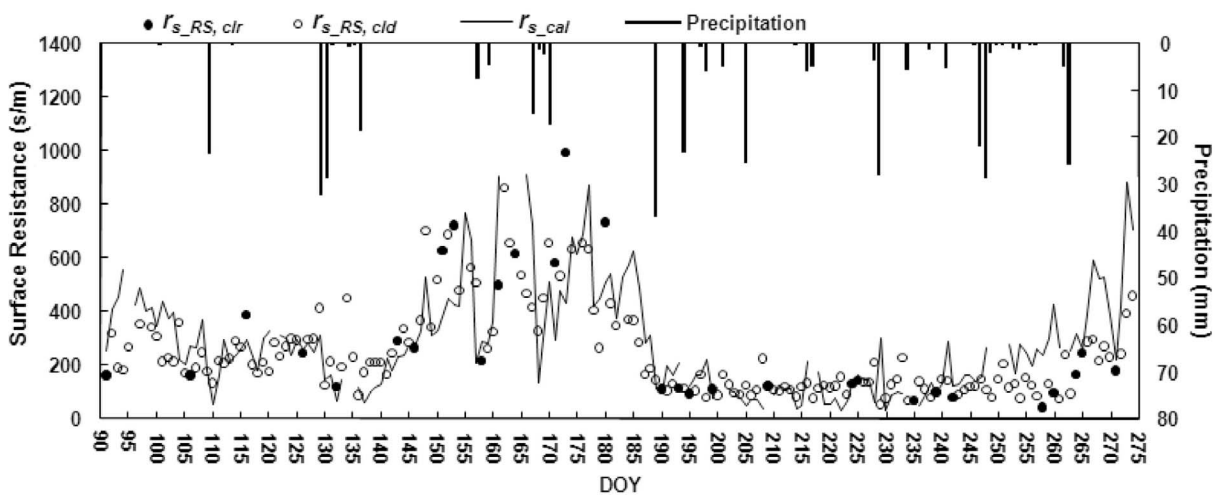


Figure 12. Comparison of the remotely sensed surface resistance and the ground-based calculation during growing seasons. (Guantao site, DOY 90–275, 2009) The solid circle represents the surface resistance on clear sky days ($r_{s_RS,clr}$) derived from the daily remote sensing evapotranspiration; the hollow circle represents the interpolated surface resistance on cloudy days ($r_{s_RS,cld}$); the solid line represents the surface resistance calculated from the ground-based data (r_{s_cal}); and the bar on the top represents the precipitation.

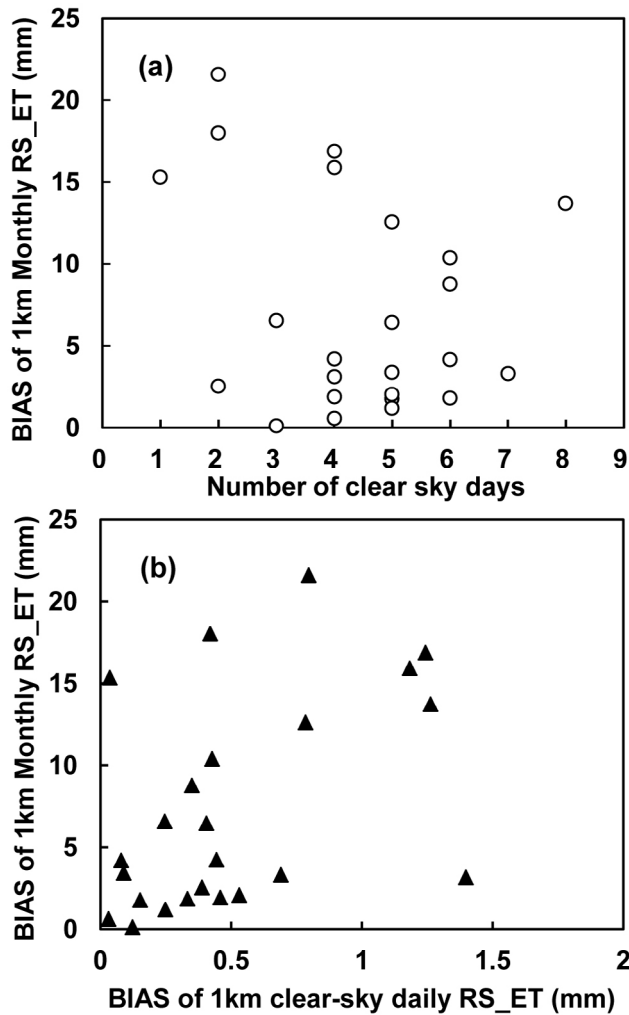


Figure 13. Relationships between the bias of 1 km monthly remote sensing evapotranspiration (RS_ET) and (a) the number of clear sky days and (b) the bias of 1 km daily RS_ET on clear sky days during the corresponding month (Guantao site, 2008–2009).

in the estimation of $r_{s,RS}$, the fluctuation of $r_{s,RS}$ was not so obvious and its accuracy was relatively poor during this period.

[48] Moreover, illustrated as Figure 13, the increasing deviation of monthly RS_ET suffered from the reduction of the number of clear sky days and the increasing bias of the daily RS_ET on clear sky days.

[49] In summary, the estimated accuracy of the 1 km monthly RS_ET was determined by the comprehensive influences of the performance in the daily RS_ET estimation on both clear and cloudy days as well as the number of clear sky days. While the daily RS_ET were mainly affected by the assumption of the constant evaporative fraction, the gap-filled performance of the daily RS_ET on cloudy days mainly depended on the meteorological elements and surface resistance. Specifically, as the daily RS_ET on cloudy days was also influenced by the estimates on clear sky days, improving the accuracy of the daily RS_ET on clear sky

days was the best way to improve the estimation of the monthly RS_ET.

4.3. Problems in the Validation Process

[50] The last aspect of the validation ought to focus on the uncertainty analysis of the validation process. This was essential to refine the validation method by measuring the uncertainties in the validation process itself. In this study, we just analyzed the problems existed in the validation process here. First, the observation errors of instruments and deviations among the different data processing methods were the two major aspects of uncertainties in the validation process. For example, the observation error of net radiation (CNR-1) was approximately 20 Wm^{-2} [Kohsiek et al., 2007], and the observation error of sensible heat flux from EC (CSAT3/LI-7500) was approximately $10\text{--}20 \text{ Wm}^{-2}$ [Mauder et al., 2006]. Errors were also caused by different data processing procedures, such as the bias from the performance of different processing software and different interpolation methods for the missing data. A difference within 5–10% was indicated in the flux data process by various eddy covariance data processing software such as Alteddy, ECPack, Eddy-Soft, Edire, eth-flux, and TUDD [Mauder et al., 2008].

[51] Second, differences resulted from the validation pixel selection. The 30 m and 1 km monthly RS_ET derived from different pixel selection methods at the Miyun site in 2009 are compared in Figure 14. The three methods for 30 m and 1 km RS_ET involved the weighted average method based on the EC or LAS footprint, the arithmetic mean of pixels (10×10 pixels around the EC location, or 3×3 pixels around the center of the LAS path), and a single pixel value (around the EC location, or the center of the LAS path). The RS_ET acquired by using the weighted average method based on the EC and LAS footprint differed from the other two methods, with relative deviations of 7.79% and 3.03% at 30 m resolution and 5.48% and 1.41% at 1 km resolution, respectively.

[52] In addition, the geometric accuracy of satellite images affected the validation results. Especially during the process of overlapping the flux source area distribution to the remote sensing image, it was essential to ensure that they completely overlapped. Moreover, pixel drift still existed in the satellite images even after the geometric correction, and the direction of drift was uncertain. These factors would introduce some uncertainties of the geometric position in the validation process.

5. Discussion and Conclusions

[53] Study on the validation method of RS_ET is an essential part of the research on the improvement of remote sensing models and the evaluation of RS_ET products. For this purpose, an innovative approach on RS_ET validation was proposed in this study. In situ measurements at different scales from the LAS and EC over the typical landscapes, along with the basin-scale water balance data, precipitation data, MODIS products, and the land use map, composed the multisource validation data, which can be used in the validations for different temporal-scale (e.g., annual, monthly, and daily) RS_ET at diverse resolutions. A relatively systematic procedure was involved in our validation, so the

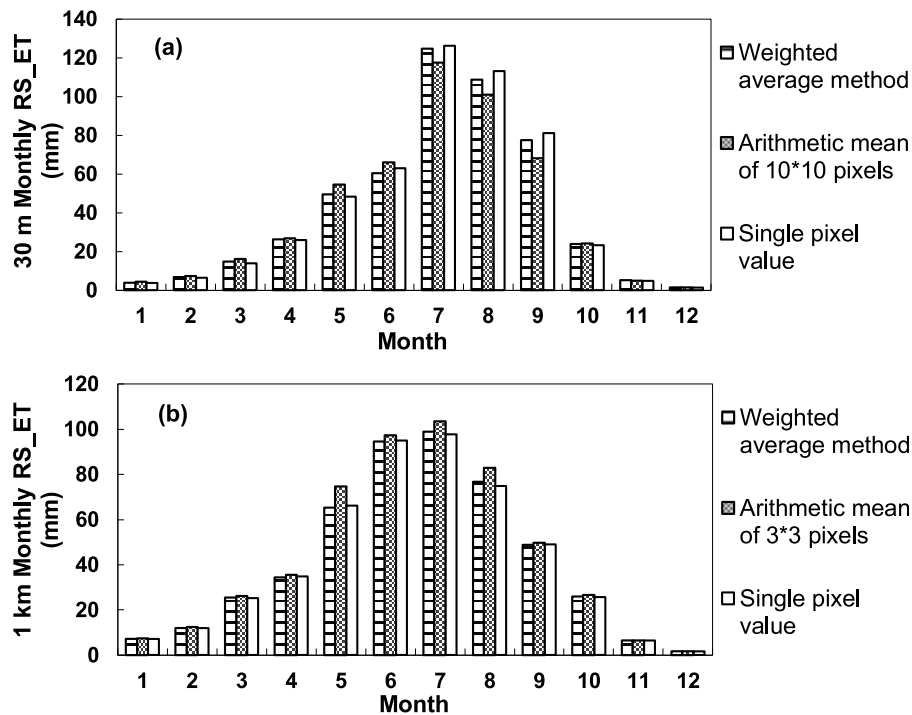


Figure 14. Comparisons of (a) 30 m and (b) 1 km monthly remote sensing evapotranspiration (RS_ET) calculated by different methods of validation pixel selection (Miyun site, 2009).

RS_ET could be evaluated on the overall accuracy and characteristics of the spatiotemporal distribution at both the basin and local scales. The error sources of RS_ET and uncertainties of the validation process could be analyzed as well.

[54] Ground-based measurements have been widely accepted in the RS_ET validation. Some validations were presented based on EC measurements, which were regarded as the most reliable measurements of fluxes [Glenn *et al.*, 2011; Mu *et al.*, 2011]. Others took the advantages of LAS measurements in the validation, which had emerged as the unique possibility of measuring path-averaged fluxes over heterogeneous land surfaces [Li *et al.*, 2009; Brunsell *et al.*, 2011]. Considering their own advantages, we utilized an observational system consisted of EC and LAS for measuring multiscale ET simultaneously in this study, and it provided a more feasible way to evaluate the RS_ET at diverse resolutions. Additionally, since the direct comparison between the in situ measurements and RS_ET derived from a satellite pixel may not be a valid comparison [Chávez *et al.*, 2005; Li *et al.*, 2008; Brunsell *et al.*, 2011], the exploration of validation pixel selection with the footprint model was investigated in detail, which could help the remotely sensed estimates to match some extent with the scale of flux measurements and made the validation more realistic than the comparison at a point scale.

[55] A case study of independent RS_ET validation was conducted over the Hai River Basin in China. A good agreement was obtained between the 1 km annual RS_ET and the water balance ET with an RMSE of 50.73 mm over this basin, and the annual RS_ET showed the consistent trend of interannual variation and spatial distribution with the validation data. This result was acceptable as an RMSE

of 118–194 mm for annual RS_ET compared to water balance ET across 26 global basins reported by Vinukollu *et al.* [2011b] was found. Vinukollu *et al.* [2011b] also indicated an RMSE of 16–35 mm and a Corr. of 0.51–0.65 for monthly RS_ET compared to 12 EC measurements. Besides, an assessment of some published validations summarized by Kalma *et al.* [2008] showed an RMSE of 0.5–1.2 mm and a Corr. of 0.81–0.96 for daily comparisons. Consequently, it indicated that the validation in this study had good results for both the 30 m and 1 km resolutions with the RMSE of 9.52–19.55 mm at monthly scale and 0.78–0.99 mm at daily scale, and had good correlation in the monthly and daily results with the Corr. of 0.84–0.87 within the expected range as well. Overall, this validation result with the MRE within 20.21% was in broad agreement with Courault *et al.* [2005], Glenn *et al.* [2007], and Verstraeten *et al.* [2008], who reported the current error of 20–30% in most regional RS_ET estimates. Furthermore, the validation results of our study had been partly involved in a report of the independent validation by Beijing Normal University for the GEF Hai River project, and had been cited by Wu *et al.* [2012]. So we concluded that the proposed validation method is reasonable and feasible.

[56] Of course, lessons should be learned from the current validation process. First, we can just obtain the ET measurement at approximate satellite pixel scale, through the multiscale flux measurements provided by EC and LAS combined with the footprint model. The spatial heterogeneity at sub-pixel scale needs to be considered, when a satellite pixel cannot be covered completely by the contributing source area over the complex landscapes. In further study, measurements from an observation matrix composed of EC and LAS, and as well as the airborne eddy covariance

observation are suggested to be carried out to develop the measured ET at the satellite pixel scale. Second, considering the spatial limitations of in situ measurements, while the remote sensing data with finer resolution, such as the Landsat TM data and airborne images has proved to be able to eliminate part of the uncertainties caused by the spatial heterogeneity [Su *et al.*, 2005; McCabe and Wood, 2006], the method for scaling the high-resolution remote sensing information to validate the RS_ET at coarse resolutions might provide an operational way. Zhang *et al.* [2010] proposed a multilevel validation strategy combined with the multiscale observations from ground, airborne to spaceborne, which can be used for the validation of the coarse-resolution RS_ET through the assessment of spaceborne-airborne-ground based ET products level-by-level after scaling. Finally, the unaccomplished problem that how to quantitatively evaluate the uncertainties of the validation process ought to be further explored.

Appendix A

[57] Appendix A shows a calculation method for the evaluation indexes. P_i is remote sensing estimates, O_i is the measured values, \bar{P} is the mean of remote sensing estimates, \bar{O} is the mean of measured values, and n is the number of samples.

[58] A series of evaluation indexes was included in the proposed validation method. The BIAS and RMSE are used to measure the differences between the estimation and measurement, the MRE and MAPE are used to measure the relative degree of their differences, and the Corr. is used to measure the consistency between them.

Mean Bias Error (BIAS):

$$BIAS = \sum_{i=1}^n (P_i - O_i) / n \quad (A1)$$

Root-Mean-Square Error (RMSE):

$$RMSE = \sqrt{\sum_{i=1}^n (P_i - O_i)^2 / n} \quad (A2)$$

Mean Relative Error (MRE):

$$MRE = \frac{100}{n} \sum_{i=1}^n \frac{P_i - O_i}{\bar{O}} \quad (A3)$$

Mean Absolute Percent Error (MAPE):

$$MAPE = \frac{100}{n} \sum_{i=1}^n \frac{|P_i - O_i|}{\bar{O}} \quad (A4)$$

Correlation Coefficient (Corr.):

$$Corr. = \sum_{i=1}^n (P_i - \bar{P})(O_i - \bar{O}) / \left[\sum_{i=1}^n (P_i - \bar{P})^2 \sum_{i=1}^n (O_i - \bar{O})^2 \right]^{1/2} \quad (A5)$$

[59] **Acknowledgments.** This work was funded by the National High Technology Research and Development Program (2012AA12A305), National Natural Science Foundation of China (40971194 and 30911130504), and Global Environment Facility (GEF) Project (TF053183). Special thanks are given to Bingfang Wu's group in the Institute of Remote Sensing Application, Chinese Academy of Sciences, for providing the RS_ET data from ETWatch system.

References

- Alavi, N., J. S. Warland, and A. A. Berg (2006), Filling gaps in evapotranspiration measurements for water budget studies: Evaluation of a Kalman filtering approach, *Agric. For. Meteorol.*, 141(1), 57–66, doi:10.1016/j.agrformet.2006.09.011.
- Allen, R. G., L. S. Pereira, D. Raes, and M. Smith (1998), Crop evapotranspiration: Guidelines for computing crop requirements, *FAO Irrig. Drain. Pap.* 56, 300 pp., Food and Agric. Org. of the U. N., Rome.
- Allen, R. G., M. Tasumi, and R. Trezza (2007), Satellite-based energy balance for mapping evapotranspiration with internalized calibration (METRIC)—Model, *J. Irrig. Drain. Eng.*, 133(4), 381–394.
- Allen, R. G., L. S. Pereira, T. A. Howell, and M. E. Jensen (2011), Evapotranspiration information reporting: I. Factors governing measurement accuracy, *Agric. Water Manage.*, 98(6), 899–920, doi:10.1016/j.agwat.2010.12.015.
- Anderson, M. C., J. M. Norman, G. R. Diak, W. P. Kustas, and J. R. Mecikalski (1997), A two-source time-integrated model for estimating surface fluxes using thermal infrared remote sensing, *Remote Sens. Environ.*, 60(2), 195–216, doi:10.1016/S0034-4257(96)00215-5.
- Bastiaanssen, W. G. M., M. Menenti, R. A. Feddes, and A. A. M. Holtslag (1998), A remote sensing surface energy balance algorithm for land (SEBAL). 1. Formulation, *J. Hydrol.*, 212–213, 198–212, doi:10.1016/S0022-1694(98)00253-4.
- Berbigier, P., J.-M. Bonnefond, and P. Mellmann (2001), CO₂ and water vapour fluxes for 2 years above Euroflux forest site, *Agric. For. Meteorol.*, 108(3), 183–197, doi:10.1016/S0168-1923(01)00240-4.
- Blyth, E. M., and R. J. Harding (1995), Application of aggregation models to surface heat flux from the Sahelian tiger bush, *Agric. For. Meteorol.*, 72(3–4), 213–235, doi:10.1016/0168-1923(94)02164-F.
- Brunsell, N. A., J. M. Ham, and K. A. Arnold (2011), Validating remotely sensed land surface fluxes in heterogeneous terrain with large aperture scintillometry, *Int. J. Remote Sens.*, 32(21), 6295–6314, doi:10.1080/01431161.2010.508058.
- Brutacart, W. (1982), *Evaporation into the Atmosphere, Theory, History, and Applications*, 299 pp., D. Reidel, Dordrecht, Netherlands.
- Businger, J. A., J. C. Wyngaard, Y. Izumi, and E. E. Bradley (1971), Flux-profile relationships in the atmospheric surface layer, *J. Atmos. Sci.*, 28, 181–189, doi:10.1175/1520-0469(1971)028<0181:FPRITA>2.0.CO;2.
- Chávez, J. L., C. M. U. Neale, L. E. Hipps, J. H. Prueger, and W. P. Kustas (2005), Comparing aircraft-based remotely sensed energy balance fluxes with eddy covariance tower data using heat flux source area functions, *J. Hydrometeorol.*, 6(6), 923–940, doi:10.1175/JHM467.1.
- Courault, D., B. Seguin, and A. Olioso (2005), Review on estimation of evapotranspiration from remote sensing data: From empirical to numerical modeling approaches, *Irrig. Drain. Syst.*, 19(3–4), 223–249, doi:10.1007/s10795-005-5186-0.
- Di Bella, C. M., C. M. Rebella, and J. M. Paruelo (2000), Evapotranspiration estimates using NOAA AVHRR imagery in the Pampa region of Argentina, *Int. J. Remote Sens.*, 21, 791–797, doi:10.1080/014311600210579.
- Falge, E., et al. (2001), Gap filling strategies for defensible annual sums of net ecosystem exchange, *Agric. For. Meteorol.*, 107(1), 43–69, doi:10.1016/S0168-1923(00)00225-2.
- Ferguson, C. R., J. Sheffield, E. F. Wood, and H. L. Gao (2010), Quantifying uncertainty in a remote sensing-based estimate of evapotranspiration over continental USA, *Int. J. Remote Sens.*, 31(14), 3821–3865, doi:10.1080/01431161.2010.483490.
- Fisher, J. B., R. J. Whittaker, and Y. Malhi (2011), ET come home: Potential evapotranspiration in geographical ecology, *Global Ecol. Biogeogr.*, 20(1), 1–18, doi:10.1111/j.1466-8238.2010.00578.x.
- French, A. N., et al. (2005), Surface energy fluxes with the Advanced Spaceborne Thermal Emission and Reflection radiometer (ASTER) at the Iowa 2002 SMACEX site (USA), *Remote Sens. Environ.*, 99(1–2), 55–65, doi:10.1016/j.rse.2005.05.015.
- Gao, Y., and D. Long (2008), Intercomparison of remote sensing-based models for estimation of evapotranspiration and accuracy assessment based on SWAT, *Hydrol. Processes*, 22, 4850–4869, doi:10.1002/hyp.7104.
- Gao, F., J. Masek, M. Schwaller, and F. Hall (2006), On the blending of the Landsat and MODIS surface reflectance: Predicting daily Landsat surface

- reflectance, *IEEE Trans. Geosci. Remote Sens.*, 44(8), 2207–2218, doi:10.1109/TGRS.2006.872081.
- Glenn, E. P., A. R. Huete, P. L. Nagler, K. K. Hirschboeck, and P. Brown (2007), Integrating Remote Sensing and Ground Methods to Estimate Evapotranspiration, *Crit. Rev. Plant Sci.*, 26(3), 139–168, doi:10.1080/07352680701402503.
- Glenn, E. P., T. M. Doody, J. P. Guerschman, A. R. Huete, E. A. King, T. R. McVicar, A. I. J. M. Van Dijk, T. G. Van Niel, M. Yebra, and Y. Zhang (2011), Actual evapotranspiration estimation by ground and remote sensing methods: The Australian experience, *Hydrol. Processes*, 25(26), 4103–4116, doi:10.1002/hyp.8391.
- Hemakumara, H. M., L. Chandrapala, and A. F. Moene (2003), Evapotranspiration fluxes over mixed vegetation areas measured from large aperture scintillometer, *Agric. Water Manage.*, 58(2), 109–122, doi:10.1016/S0378-3774(02)00131-2.
- Hoedjes, J. C. B., A. Chehbouni, J. Ezzahar, R. Escadafal, and H. A. R. De Bruin (2007), Comparison of large aperture scintillometer and eddy covariance measurements: Can thermal infrared data be used to capture footprint-induced differences?, *J. Hydrometeorol.*, 8(2), 144–159, doi:10.1175/JHM561.1.
- Hoedjes, J. C. B., A. Chehbouni, F. Jacob, J. Ezzahar, and G. Boulet (2008), Deriving daily evapotranspiration from remotely sensed instantaneous evaporative fraction over olive orchard in semi-arid Morocco, *J. Hydrol.*, 354(1–4), 53–64, doi:10.1016/j.jhydrol.2008.02.016.
- Jackson, R. D., R. J. Reginato, and S. B. Idso (1977), Wheat canopy temperature: A practical tool for evaluating water requirements, *Water Resour. Res.*, 13(3), 651–656, doi:10.1029/WR013i003p0651.
- Jia, L., Z. B. Su, B. van den Hurk, M. Menenti, A. Moene, H. A. R. De Bruin, J. J. B. Yrisarry, M. Ibanez, and A. Cuesta (2003), Estimation of sensible heat flux using the Surface Energy Balance System (SEBS) and ATSR measurements, *Phys. Chem. Earth*, 28(1–3), 75–88.
- Jiang, L., and S. Islam (1999), A methodology for estimation of surface evapotranspiration over large areas using remote sensing observations, *Geophys. Res. Lett.*, 26(17), 2773–2776, doi:10.1029/1999GL006049.
- Jiang, L., and S. Islam (2001), Estimation of surface evaporation map over Southern Great Plains using remote sensing data, *Water Resour. Res.*, 37(2), 329–340, doi:10.1029/2000WR900255.
- Jiménez, C., et al. (2011), Global intercomparison of 12 land surface heat flux estimates, *J. Geophys. Res.*, 116, D02102, doi:10.1029/2010JD014545.
- Kalma, J., T. McVicar, and M. McCabe (2008), Estimating land surface evaporation: A review of methods using remotely sensed surface temperature data, *Surv. Geophys.*, 29(4–5), 421–469, doi:10.1007/s10712-008-9037-z.
- Kleissl, J., S. H. Hong, and J. M. H. Hendrickx (2009), New Mexico scintillometer network: Support of remote sensing and hydrologic and meteorological models, *Bull. Am. Meteorol. Soc.*, 90(2), 207–218, doi:10.1175/2008BAMS2480.1.
- Kohsiek, W., C. Liebethal, T. Foken, R. Vogt, S. P. Oncley, C. Bernhofer, and H. A. R. Debruin (2007), The energy balance experiment EBEX-2000. Part III: Behaviour and quality of the radiation measurements, *Boundary Layer Meteorol.*, 123(1), 55–75, doi:10.1007/s10546-006-9135-8.
- Kormann, R., and F. Meixner (2001), An analytical footprint model for non-neutral stratification, *Boundary Layer Meteorol.*, 99(2), 207–224, doi:10.1023/A:1018991015119.
- Li, F., W. P. Kustas, M. C. Anderson, J. H. Prueger, and R. L. Scott (2008), Effect of remote sensing spatial resolution on interpreting tower-based flux observations, *Remote Sens. Environ.*, 112(2), 337–349, doi:10.1016/j.rse.2006.11.032.
- Li, Z.-L., R. Tang, Z. Wan, Y. Bi, C. Zhou, B. Tang, G. Yan, and X. Zhang (2009), A review of current methodologies for regional evapotranspiration estimation from remotely sensed data, *Sensors*, 9(5), 3801–3853, doi:10.3390/s90503801.
- Liu, S. F., J. Xiong, and B. F. Wu (2011), ETWatch: A method of multi-resolution ET data fusion [in Chinese with English abstract], *J. Remote Sens.*, 15(2), 255–269.
- Liu, S. M., R. Sun, Z. P. Sun, X. O. Li, and C. M. Liu (2006), Evaluation of three complementary relationship approaches for evapotranspiration over the Yellow River basin, *Hydrol. Processes*, 20(11), 2347–2361, doi:10.1002/hyp.6048.
- Liu, S. M., G. Hu, L. Lu, and D. F. Mao (2007a), Estimation of regional evapotranspiration by TM/ETM plus data over heterogeneous surfaces, *Photogramm. Eng. Remote Sens.*, 73(10), 1169–1178.
- Liu, S. M., L. Lu, D. F. Mao, and L. Jia (2007b), Evaluating parameterizations of aerodynamic resistance to heat transfer using field measurements, *Hydrol. Earth Syst. Sci.*, 11, 769–783, doi:10.5194/hess-11-769-2007.
- Liu, S. M., J. Bai, Z. Jia, L. Jia, H. Zhou, and L. Lu (2010a), Estimation of evapotranspiration in the Mu Us Sandland of China, *Hydrol. Earth Syst. Sci.*, 14(3), 573–584, doi:10.5194/hess-14-573-2010.
- Liu, S. M., X. Li, S. Shi, Z. Xu, J. Bai, X. Ding, Z. Jia, and M. Zhu (2010b), Measurement, analysis and application of surface energy and water vapor fluxes at larger scale [in Chinese with English abstract], *Adv. Earth Sci.*, 25(11), 1113–1127.
- Liu, S. M., Z. W. Xu, W. Z. Wang, Z. Z. Jia, M. J. Zhu, J. Bai, and J. M. Wang (2011), A comparison of eddy-covariance and large aperture scintillometer measurements with respect to the energy balance closure problem, *Hydrol. Earth Syst. Sci.*, 15, 1291–1306, doi:10.5194/hess-15-1291-2011.
- Marx, A., H. Kunstmann, D. Schuttemeyer, and A. F. Moene (2008), Uncertainty analysis for satellite derived sensible heat fluxes and scintillometer measurements over Savannah environment and comparison to mesoscale meteorological simulation results, *Agric. For. Meteorol.*, 148(4), 656–667, doi:10.1016/j.agrformet.2007.11.009.
- Mauder, M., C. Liebethal, M. Gockede, J. P. Leps, F. Beyrich, and T. Foken (2006), Processing and quality control of flux data during LITFASS-2003, *Boundary Layer Meteorol.*, 121(1), 67–88, doi:10.1007/s10546-006-9094-0.
- Mauder, M., T. Foken, R. Clement, J. A. Elbers, W. Eugster, T. Grunwald, B. Heusinkveld, and O. Kolle (2008), Quality control of CarboEurope flux data - Part 2: Inter-comparison of eddy-covariance software, *Biogeosciences*, 5(2), 451–462, doi:10.5194/bg-5-451-2008.
- McCabe, M. F., and E. F. Wood (2006), Scale influences on the remote estimation of evapotranspiration using multiple satellite sensors, *Remote Sens. Environ.*, 105(4), 271–285, doi:10.1016/j.rse.2006.07.006.
- Meijninger, W. M. L., A. E. Green, O. K. Hartogensis, W. Kohsiek, J. C. B. Hoedjes, R. M. Zuurbier, and H. A. R. De Bruin (2002a), Determination of area-averaged water vapour fluxes with large aperture and radio wave scintillometers over a heterogeneous surface—Flevoland field experiment, *Boundary Layer Meteorol.*, 105(1), 63–83, doi:10.1023/A:1019683616097.
- Meijninger, W. M. L., O. K. Hartogensis, W. Kohsiek, J. C. B. Hoedjes, R. M. Zuurbier, and H. A. R. De Bruin (2002b), Determination of area-averaged sensible heat fluxes with a large aperture scintillometer over a heterogeneous surface—Flevoland field experiment, *Boundary Layer Meteorol.*, 105(1), 37–62, doi:10.1023/A:1019647732027.
- Miralles, D. G., T. R. H. Holmes, R. A. M. De Jeu, J. H. Gash, A. G. C. A. Meesters, and A. J. Dolman (2011), Global land-surface evaporation estimated from satellite-based observations, *Hydrol. Earth Syst. Sci.*, 15(2), 453–469, doi:10.5194/hess-15-453-2011.
- Monteith, J. L. (1965), Evaporation and environment, in *The State and Movement of Water in Living Organisms, Symp. Soc. Exp. Biol.*, vol. 19, edited by G. E. Fogg, pp. 205–234, Academic, New York.
- Mu, Q., F. A. Heinsch, M. Zhao, and S. W. Running (2007), Development of a global evapotranspiration algorithm based on MODIS and global meteorology data, *Remote Sens. Environ.*, 111(4), 519–536, doi:10.1016/j.rse.2007.04.015.
- Mu, Q., M. Zhao, and S. W. Running (2011), Improvements to a MODIS global terrestrial evapotranspiration algorithm, *Remote Sens. Environ.*, 115(8), 1781–1800, doi:10.1016/j.rse.2011.02.019.
- Mueller, B., et al. (2011), Evaluation of global observations-based evapotranspiration datasets and IPCC AR4 simulations, *Geophys. Res. Lett.*, 38, L06402, doi:10.1029/2010GL046230.
- Nagler, P. (2011), The role of remote sensing observations and models in hydrology: The science of evapotranspiration, *Hydrol. Processes*, 25(26), 3977–3978, doi:10.1002/hyp.8436.
- Norman, J. M., W. P. Kustas, and K. S. Humes (1995), Source approach for estimating soil and vegetation energy fluxes in observations of directional radiometric surface temperature, *Agric. For. Meteorol.*, 77(3–4), 263–293, doi:10.1016/0168-1923(95)02265-Y.
- Paulson, C. A. (1970), The mathematical representation of wind speed and temperature profiles in the unstable atmospheric surface layer, *J. Appl. Meteorol.*, 9(6), 857–861, doi:10.1175/1520-0450(1970)009<0857:TMROWS>2.0.CO;2.
- Rymph, S. J. (2004), Modeling growth and composition of perennial tropical forage grasses, PhD thesis, 330 pp., Univ. of Fla., Gainesville.
- Shuttleworth, W. J., and R. J. Gurney (1990), The theoretical relationship between foliage temperature and canopy resistance in sparse crops, *Q. J. R. Meteorol. Soc.*, 116(492), 497–519, doi:10.1002/qj.49711649213.
- Song, Y., J. Wang, K. Yang, M. Ma, X. Li, Z. H. Zhang, and X. F. Wang (2012), A revised surface resistance parameterisation for estimating latent heat flux from remotely sensed data, *Int. J. Appl. Earth Obs. Geoinf.*, 17, 76–84, doi:10.1016/j.jag.2011.10.011.

- Su, Z. (2002), The Surface Energy Balance System (SEBS) for estimation of turbulent heat fluxes, *Hydrol. Earth Syst. Sci.*, 6(1), 85–100, doi:10.5194/hess-6-85-2002.
- Su, H., M. F. McCabe, E. F. Wood, Z. Su, and J. H. Prueger (2005), Modeling Evapotranspiration during SMACEX: Comparing two approaches for local- and regional-scale prediction, *J. Hydrometeorol.*, 6(6), 910–922, doi:10.1175/JHM466.1.
- Tang, R., Z.-L. Li, and B. Tang (2010), An application of the Ts-VI triangle method with enhanced edges determination for evapotranspiration estimation from MODIS data in arid and semi-arid regions: Implementation and validation, *Remote Sens. Environ.*, 114(3), 540–551, doi:10.1016/j.rse.2009.10.012.
- Tang, R., Z.-L. Li, Y. Jia, C. Li, X. Sun, W. P. Kustas, and M. C. Anderson (2011), An intercomparison of three remote sensing-based energy balance models using Large Aperture Scintillometer measurements over a wheat-corn production region, *Remote Sens. Environ.*, 115(12), 3187–3202, doi:10.1016/j.rse.2011.07.004.
- Tasumi, M., R. Trezza, R. G. Allen, and J. L. Wright (2005), Operational aspects of satellite-based energy balance models for irrigated crops in the semi-arid U.S., *Irrig. Drain. Syst.*, 19(3–4), 355–376, doi:10.1007/s10795-005-8138-9.
- Teixeira, A. H. D. C., W. G. M. Bastiaanssen, M. D. Ahmad, and M. G. Bos (2009), Reviewing SEBAL input parameters for assessing evapotranspiration and water productivity for the Low-Middle Sao Francisco River basin, Brazil Part B: Application to the regional scale, *Agric. For. Meteorol.*, 149(3–4), 477–490, doi:10.1016/j.agrformet.2008.09.014.
- Thom, A. S. (1975), Momentum, mass and heat exchange of plant communities, in *Vegetation and the Atmosphere*, edited by J. L. Monteith, pp. 57–109, Academic, London.
- Timmermans, W. J., W. P. Kustas, M. C. Anderson, and A. N. French (2007), An intercomparison of the Surface Energy Balance Algorithm for Land (SEBAL) and the Two-Source Energy Balance (TSEB) modeling schemes, *Remote Sens. Environ.*, 108(4), 369–384, doi:10.1016/j.rse.2006.11.028.
- Twine, T. E., W. P. Kustas, J. M. Norman, D. R. Cook, P. R. Houser, T. P. Meyers, J. H. Prueger, P. J. Starks, and M. L. Wesely (2000), Correcting eddy-covariance flux underestimates over a grassland, *Agric. For. Meteorol.*, 103(3), 279–300, doi:10.1016/S0168-1923(00)00123-4.
- Verstraeten, W., F. Veroustraete, and J. Feyen (2008), Assessment of Evapotranspiration and Soil Moisture Content Across Different Scales of Observation, *Sensors*, 8(1), 70–117, doi:10.3390/s8010070.
- Vinukollu, R. K., R. Meynadier, J. Sheffield, and E. F. Wood (2011a), Multi-model, multi-sensor estimates of global evapotranspiration: Climatology, uncertainties and trends, *Hydrol. Processes*, 25(26), 3993–4010, doi:10.1002/hyp.8393.
- Vinukollu, R. K., E. F. Wood, C. R. Ferguson, and J. B. Fisher (2011b), Global estimates of evapotranspiration for climate studies using multi-sensor remote sensing data: Evaluation of three process-based approaches, *Remote Sens. Environ.*, 115(3), 801–823, doi:10.1016/j.rse.2010.11.006.
- Wang, K. C., and R. E. Dickinson (2012), A review of global terrestrial evapotranspiration: Observation, modeling, climatology, and climatic variability, *Rev. Geophys.*, 50, RG2005, doi:10.1029/2011RG000373.
- Wang, K. C., and S. L. Liang (2008), An improved method for estimating global evapotranspiration based on satellite determination of surface net radiation, vegetation index, temperature, and soil moisture, *J. Hydrometeorol.*, 9(4), 712–727, doi:10.1175/2007JHM911.1.
- Wang, K. C., Z. Li, and M. Cribb (2006), Estimation of evaporative fraction from a combination of day and night land surface temperatures and NDVI: A new method to determine the Priestley-Taylor parameter, *Remote Sens. Environ.*, 102(3–4), 293–305, doi:10.1016/j.rse.2006.02.007.
- Watts, C. J., A. Chehbouni, J. C. Rodriguez, Y. H. Kerr, O. Hartogensis, and H. A. R. de Bruin (2000), Comparison of sensible heat flux estimates using AVHRR with scintillometer measurements over semi-arid grassland in northwest Mexico, *Agric. For. Meteorol.*, 105(1–3), 81–89, doi:10.1016/S0168-1923(00)00188-X.
- Webb, E. K. (1970), Profile relationships: The log-linear range, and extension to strong stability, *Q. J. R. Meteorol. Soc.*, 96(407), 67–90, doi:10.1002/qj.49709640708.
- Wesely, M. L. (1976), The combined effect of temperature and humidity fluctuations on refractive index, *J. Appl. Meteorol.*, 15, 43–49, doi:10.1175/1520-0450(1976)015<0043:TCEOTA>2.0.CO;2.
- Wu, B. F., J. Xiong, and N. N. Yan (2011), ETWatch: Models and methods [in Chinese with English abstract], *J. Remote Sens.*, 15(2), 224–239.
- Wu, B. F., N. N. Yan, J. Xiong, W. G. M. Bastiaanssen, W. W. Zhu, and A. Stein (2012), Validation of ETWatch using field measurements at diverse landscapes: A case study in Hai Basin of China, *J. Hydrol.*, 436–437, 67–80, doi:10.1016/j.jhydrol.2012.02.043.
- Xiong, J., B. F. Wu, N. N. Yan, Y. Zeng, and S. F. Liu (2010), Estimation and validation of land surface evaporation using remote sensing and meteorological data in north China, *IEEE J. Sel. Top. Appl. Earth Obs. Remote Sens.*, 3(3), 337–344, doi:10.1109/JSTARS.2010.2040806.
- Yang, K., and J. Wang (2008), A temperature prediction-correction method for estimating surface soil heat flux from soil temperature and moisture data, *Sci. China Earth Sci.*, 51(5), 721–729, doi:10.1007/s11430-008-0036-1.
- Yang, K., T. Koike, and D. W. Yang (2003), Surface flux parameterization in the Tibetan Plateau, *Boundary Layer Meteorol.*, 106(2), 245–262, doi:10.1023/A:1021152407334.
- Yuan, Z., Y. Shen, Y. Chu, and Y. Qi (2009), Variations and distribution of temperature and precipitation of Haihe River Basin in recent 40 years [in Chinese with English abstract], *Res. Soil Water Conserv.*, 16(3), 24–26.
- Zhang, R. H., J. Tian, Z. L. Li, H. B. Su, S. H. Chen, and X. Z. Tang (2010), Principles and methods for the validation of quantitative remote sensing products, *Sci. China Earth Sci.*, 53(5), 741–751, doi:10.1007/s11430-010-0021-3.